Master course in *"Industrial Chemistry"*

Master Degree in
*"**Low Carbon Technology and Environmental Chemistry**"*

TITLE:

"A-Site Cation Engineering of Tin Halide Perovskite Solar Cells"

DANDIDATE:
Edoardo Albanesi
Matricola: 0001097595

SUPERVISOR:
Daniele Cortecchia (UNIBO)

CO-SUPERVISORS:
Isabella Poli (IIT)
Annamaria Petrozza (IIT)

January 2025
Academic year 2023-2024

“What an exceptional source of energy is solar energy! Let's hope we don't have to wait for the exhaustion of oil and coal to exploit it.”

Thomas A. Edison - 1931

i. Abstract

Metal halide perovskites are a class of materials that have gained significant attention in the field of thin film photovoltaics in recent years due to their exceptional optoelectronic properties. Among all, tin halide perovskites (chemical formula $ASnX_3$, with A= methylammonium MA^+, formamidinium FA^+ or cesium Cs^+ and X= iodide I^- and/or bromide Br^-) have gained much attention thanks to their low bandgap of 1.4 eV, which is close to the ideal bandgap for single-junction devices according to the Shockley-Quessier limit. Despite the promise, their power conversion efficiency has not reached levels comparable to traditional silicon and lead-based solar cells (>25%). The main reason lies in the soft nature of the tin-halide lattice and the facile oxidation of tin(II) to tin(IV), which induce relatively low defect formation energies and cause a severe intrinsic p-doping that limits the power conversion efficiencies in devices. The p-doping can severely change depending on the chemical composition of the material itself, for example, it can be reduced by changing the stoichiometry of the material enriching it with Sn or changing the X-site anion.

Less is known about the effect of the A-site cation. The project aims at exploring the relationship between the A-site composition and optoelectronic, structural and morphological properties of tin halide perovskite thin films produced via solution process to further optimize them as absorber materials and integrate them into photovoltaic solar cells. We found that films with different cations exhibit high p-doping concentrations but distinct structural properties and markedly different morphologies, significantly affecting charge transport properties. More compact films with larger grains demonstrated higher effective charge carrier mobility and conductivity. Through careful optimization of the spin-coating process, we were able to achieve comparable conductivity values across different compositions. This study emphasizes the critical role of film quality in determining electronic properties and provides insights for improving tin perovskite solar cell performance.

ii. Abstract in Italian

Le perovskiti alogene metalliche sono una classe di materiali che hanno attirato molta attenzione nel campo dei fotovoltaici a film sottile negli ultimi anni grazie alle loro eccezionali proprietà optoelettroniche. Tra queste, le perovskiti a stagno (formula chimica $ASnX_3$, con A = metilammonio MA^+, formamidinio FA^+ o cesio Cs^+ e X = ioduro I^- e/o bromuro Br^-) hanno suscitato particolare interesse grazie al loro basso gap energetico di 1,4 eV, che si avvicina al gap ideale per dispositivi a giunzione singola secondo il limite di Shockley-Queisser. Nonostante il loro grande potenziale, l'efficienza di conversione della potenza non ha ancora raggiunto livelli comparabili a quelli delle celle solari tradizionali al silicio e al piombo (>25%). La principale ragione risiede nella natura morbida della matrice alogeno-stagno e nell'ossidazione facile dello stagno (II) a stagno (IV), che inducono energie di formazione dei difetti relativamente basse e causano un forte p-doping intrinseco, limitando così l'efficienza di conversione della potenza nei dispositivi. Le proprietà optoelettroniche dei semiconduttori a base di stagno sono fortemente influenzate dal p-doping, che può variare notevolmente a seconda della composizione chimica del materiale stesso. Ad esempio, il p-doping del materiale può essere ridotto cambiando la stechiometria del materiale, arricchendolo di stagno, o modificando l'anione del sito X.

Meno è noto riguardo agli effetti del catione del sito A. Il progetto si propone di esplorare la relazione tra la composizione del sito A e le proprietà optoelettroniche, strutturali e morfologiche dei film sottili di perovskite al stagno prodotti tramite un processo a soluzione, al fine di ottimizzarli ulteriormente come materiali assorbitori e integrarli nelle celle solari fotovoltaiche. Abbiamo scoperto che, anche se i film finali presentano proprietà differenti intrinseche ai cationi utilizzati, la morfologia del film può essere controllata grazie all'uso di più tecniche di deposizione e che una struttura simile del film può ridurre significativamente le differenze di proprietà nei film finali di perovskite.

iii. List of Figures

iv. List of Abbreviation

PV = *Photovoltaic*

MHPs = *Metal Halide Perovskites*

FAI = *Formamidinium Iodide*

MAI = *Metilammonium Iodide*

CsI = *Cesium Iodide*

TH = *Tin Halide*

THPs = *Tin Halide Perovskites*

LHPs = *Lead Halide Perovskites*

SCs = *Solar Cells*

HPSCs = *Halide Perovskite Solar Cells*

TPSCs =*Tin Perovskite Solar Cells.*

OLEDs = *Organic Light-Emitting Diodes*

PSCs = *Perovskite Solar Cells*

CBM = *Conductive Band Minimum*

VBM = *Valence Band Maximum*

ETL = *Electrons Transport Layer*

HTL = *Hole Transport Layer*

TCO = *Transparent Conductive Oxide*

XRD = *X-Ray Diffraction*

SEM = *Scanning Electrons Microscope*

1. Introduction

The growing world population is driving up energy demand. With the advancement in technology, the global need for electricity has reached unprecedented level and will continue to increase. As the Unites States Energy Information highlights, an increase of 40% in global energy consumption will occur by the year 2040 *[1][2]*. Fossil fuels are considered nowadays the major energy source, but they are depleting rapidly and moreover their use mostly implies the production of carbon dioxide and other greenhouse gasses that have a major role in global warming trapping the heat in the environment.

The quest for alternative renewable energy source has led to significant advancement in various technological sectors. Solar, wind, geothermal, and hydrothermal are considered as a few alternatives and have drawn considerable attention. Among these, photo-voltaic (PV) technologies have emerged as a promising solution to harnessing solar energy and addressing the world's energy needs *[3].*

The potential of PV technologies lies not only in the ability to harvest the light coming from the sun and produce electricity but also in the lower amount of waste and harmful emission produced during their operation when compared to fossil fuels. As the high utilization of stock resources remains the main concern in the production of solar panels, 15% of the world energy demand in 2023 was produced by solar panels and wind turbines, share that will need to reach the 45% by 2030 to meet the requirement dictate by IPCC to contain the climate changes. Solar cells are used to translate solar energy in an usable form.

The concept of solar cell was first developed by A. E. Becquerel in 1839 but only in the 20th century more research were done and the efficiency that initially was around 1% rapidly increased to 6% and then to 10%.

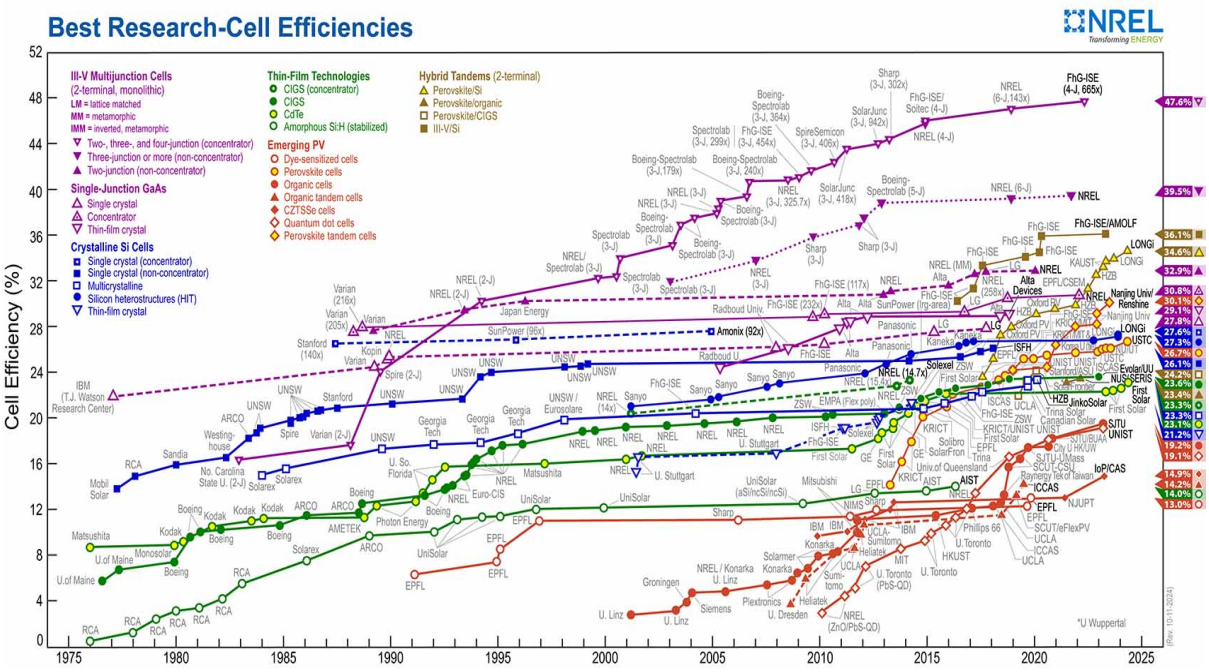

Figure 1 – Solar cells efficiency progress over the last 40 years [4].

SCs technologies may be classified in three types, known as SCs generations. The first-generation make use of crystalline silicon. They are marketed as traditional SCs and have achieved efficiencies of 26%. For the second-generation SCs thin film made of amorphous silicon (Si) and Cadmium telluride (CdTe) material are used *[5][6]*. The third-generation SCs try to overcome the problem of the previous two such as high cost of fabrication and disposal challenges. Dye-sensitize SCs, Organic SCs and Halide Perovskite Solar Cells (HPSCs) are the main representants of this generation and in the past ten years many researches were carried out to improve the outstanding theoretical properties that these technologies can offer. In the realm of photovoltaics Halide Perovskite Solar Cells (PSCs) represent one of the most exciting breakthroughs in recent years.

By modifying the deposition technologies and optimizing the perovskite film configuration the PCE was increased from a 3% up to 25.2%. Such a high value of efficiency has brought interest in further researches toward commercialization.

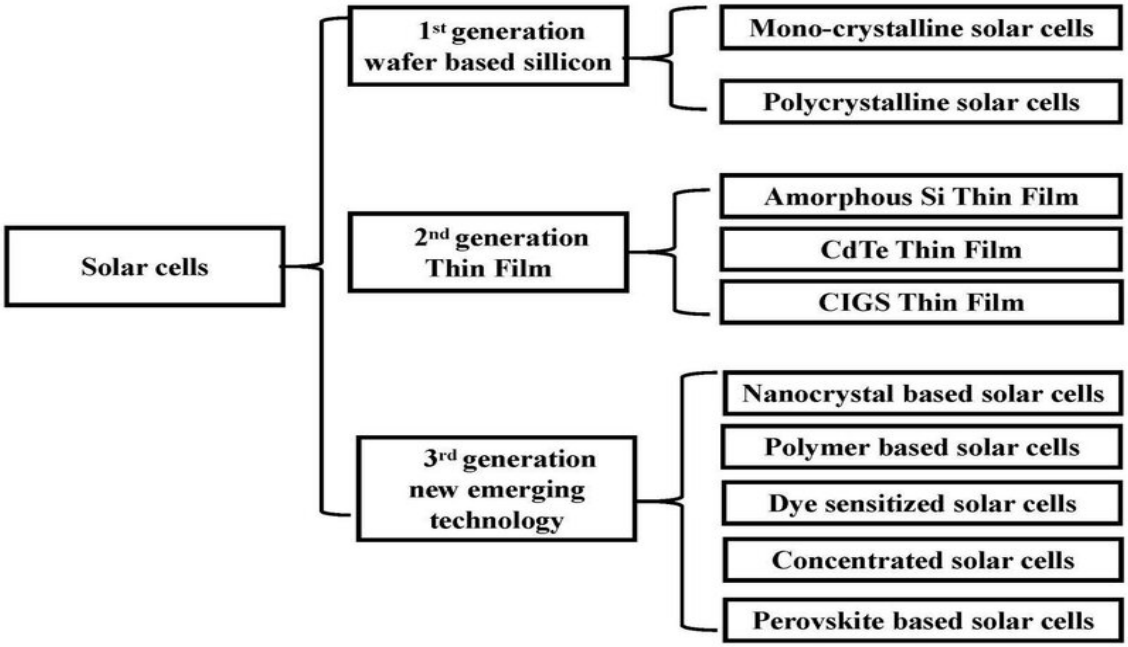

Figure 2 – Representative scheme of the three categories of solar cells from *Lu, Kunrun. (2023) [5].*

1.1. Metal Halide Perovskite.

Metal halide perovskites are a class of materials that have gained significant attention in recent years. Name after the discovery of the mineral calcium titanium oxide ($CaTiO_3$), which was found to have a distinctive crystal structure.

Figure 3 – Natural crystal of perovskite.

- ***Crystal structure***

The perovskite crystal structure comprises a minimum of three dissimilar species and have universal formula ABX_3. X is a negative anion, while A and B can be positive cation of varying magnitudes, the A site is larger in comparison to B site. To form a perovskite structure the charge neutrality condition should be followed, therefore for n that denotes the ions vacancy for A, B and X the following equation should be respected.

$$3n(X) = n(A) + n(B) \qquad (1)$$

A typically perovskite unit is showed in Figure 4 and as evident A cations , B cations and X anions arrangement consists of a cubic lattice with a central cation B, A cations surrounding it, and an octahedral arrangement of corner-sharing anions.

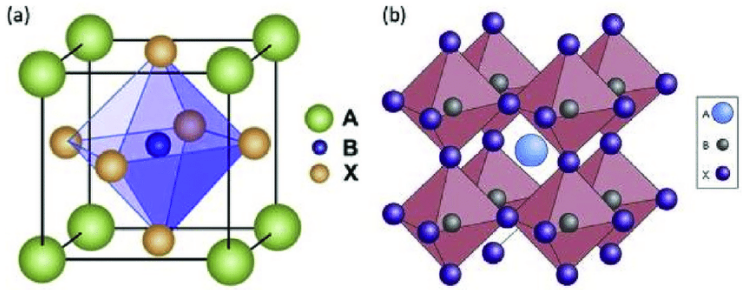

Figure 4 – Perovskite crystal structure

Tetragonal and orthorhombic structures also exist and this is because not all the combinations between cations or anions create a stable cubic 3D structure. For example, the possible dimensions of the A cation are dictated by the dimensions of the B and X ions in order to form the octahedral framework. To indicate which combination between anions and cations realizes a stable perovskite structure, two empirical parameters are used.

The first parameter is the geometrical Goldschmidt tolerance factor (*t*) defined by the Eq. 2 where Ra, Rb, and Rx are the ionic radii of the A, B, and X sites respectively.

$$\boldsymbol{t = \frac{rA + rX}{\sqrt{2}(rB + rO)}} \qquad (2)$$

Data suggests that *t* values have to be in the range between 0.8 and 1.0 to maintain a 3D perovskite structure *[8]*. Generally, a tolerance factor between 0.8 and 0.9 shows a distorted structure with rhombohedral, orthorhombic, or tetragonal symmetry; if the values are between 0.9 and 1 an ideal cubic structure can be form.

To assess the fit of the B site cation into the X6 octahedron, a second parameter called the octahedral factor (μ) is defined and is calculated following Eq. 3.

$$\mu = \frac{rB}{rX} \qquad (3)$$

Empirically determined μ values between 0.442 and 0.895 give rise to a perovskite structure.

In halide perovskites, inorganic cations like alkali metal (Cs^+, Rb^+, K^+) or organic cations like formamidinium (NH2CH = NH^{2+} or FA^+) or methylammonium ($CH3NH3^+$ or MA^+) account for A cation positions; divalent metal ions like Pb^{2+}, Sn^{2+} and Ge^{2+} account for B positions and halogens like I^-, Br^-, or Cl^- for X anion positions. High device performances are reached in lead-based perovskites. They offer attractive optoelectronic features such as strong optical absorption coefficient, high charge carrier mobility, long diffusion length, high tolerance to defects and an high open circuit voltage, with a PCE that can reach up to 25.2%. Apart from these pros LHPs have also two main drawbacks:

(i) they have poor stability towards humidity, high temperature, and illumination, due to the hygroscopic nature of the organic cations.

(ii) Lead is an hazardous element that due to its high toxicity may lead to possible harmful consequences on the human health and the environment *[9].*

These problems have forced researchers to look for substituents of lead inside the perovskite structure that are more environmentally stable and that can provide similar performance and characteristics.

1.2. Tin halide perovskite.

Tin (Sn) is the second most used metal of the 14^{14} group in the formation of perovskites. Sn-based PSCs have been able to show a PCE of more than 13% during the past years *[10]*. THPs are sensitive to ambient conditions that directly affect the efficiency of the devices and their long-term stability. Although being very promising, tin halide perovskites are not fulfilling the expectations. In practice Sn^{2+} has an oxidation tendency towards Sn^{4+}, which causes intrinsic hole doping within the material, leading to high recombination rate within the film, short carrier lifetime, in the range of few ns, and consequently short diffusion length (10-100nm) *[11]*.

Many strategies have been adopted to reduce tin oxidation, for example using additives such as SnF_2 or through solvent engineering. Compositional engineering is one of the most effective approaches to tailor the optoelectronic properties of the THPs and impact the device stability *[12].*

- ***A-site Cation Composition.***

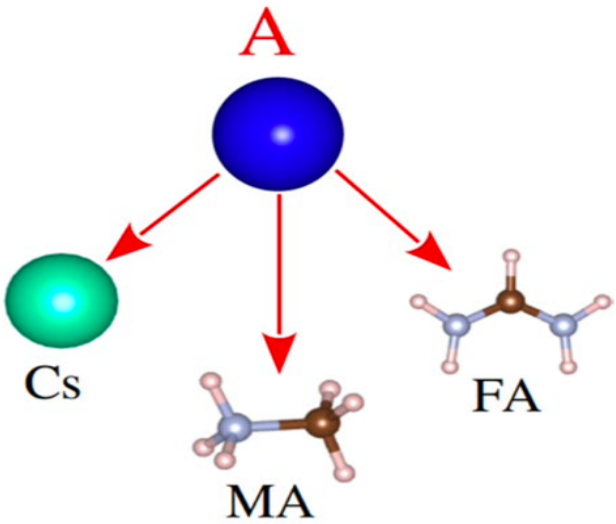

Figure 5 – A-site possible cations for Tin Halide Perovskite

In the THPs structure, the central position, occupied by an organic (MA^+, FA^+) or alkali metal (Cs^+) A site cation, heavily influences the resulting electronic properties and the intrinsic stability of the photovoltaic devices prepared with it. [13]

MA^+ (radius of 217 pm) and Cs^+ (radius of 167 pm) cations guarantee a stable perovskite phase. FA^+ (253 pm) is a little bit larger, although slight distortions within the inorganic framework will allow the formation of the perovskite structure [14].

For $MASnI_3$ a cubic structure is obtained but lowering the temperature is observe a phase transaction to the lower-symmetry tetragonal structure. For $FASnI_3$ there is not a complete understanding of the crystallographic phase, and multiple phase transition at different temperature due to the steric effect caused by the larger FA^+ cations are observed. $CsSnI_3$ shows four polymorphs, three of them show a black color while one is yellow. Decreasing the temperature from 152°C a phase transition from black cubic (B-α) to black tetragonal (B-β) phase is observe. And again a transition at 78°C to black orthorhombic phase (B-γ) is obtain. The yellow (Y) phase is characterized by a non-perovskite orthorhombic cell with 1D double-chain structure and can coexist with the B-γ orthorhombic. The yellow phase form is also obtained because of the spontaneous oxidation of Sn^{2+} to Sn^{4+} and the stress cause on the perovskite structure by oxygen and moisture *[15]*

One main difference is the thermostability of the perovskite structure in accordance to the different covalent / ionic interaction of the different cations.

The inorganic Cs^+ cation has a stronger covalent/ionic interaction with the X-site halogen anion, leading to a lower free energy and a higher thermodynamic stability. Due to this, the melting point of $CsSnI_3$ is as high as 451°C, while $MASnI_3$ and $FASnI_3$ begin to decompose at 200°C.

- ***Electronic Structure***

A major reason why the performances of tin-based perovskite are inferior to that of traditional lead-based perovskite can be ascribed to the easily oxidation of Sn^{2+} [16].

The reason for Sn^{2+} oxidization essentially relates in the difference external electron configuration of Pb^{2+} and Sn^{2+}. The lone pair electrons in 5s orbital of Sn^{2+} are relatively apt to be lost, which makes the Sn^{2+} oxidizing into Sn^{4+}. The

different electron configurations of Pb^{2+} and Sn^{2+} also makes the Lewis acidity of SnI_2 higher than PbI_2 leading to the fast reaction speed of SnI_2 with Lewis bases.

Therefore, the crystallization process of tin-based perovskite is less controllable and faster during the spin-coating process compared to lead based perovskites resulting in inhomogeneous thin films with micron-sized pinholes.

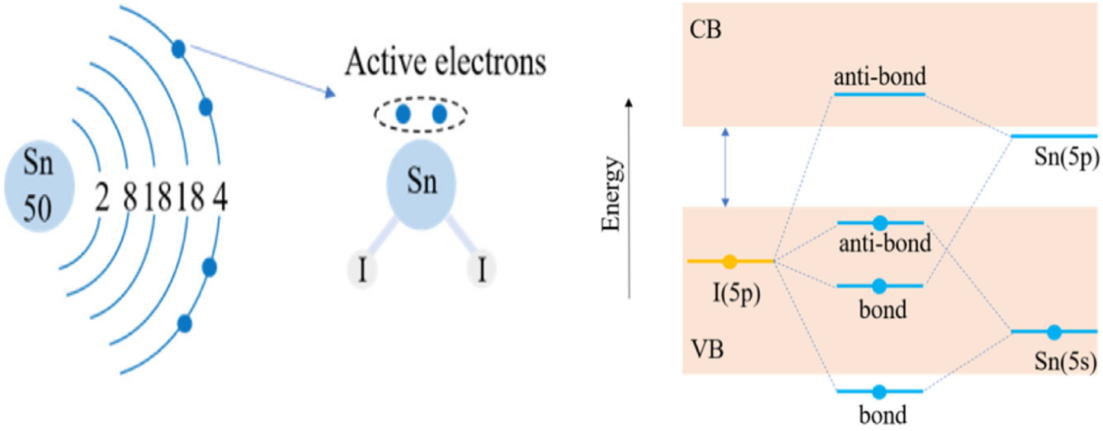

Figure 6 – Orbital illustration of Tin (left) and band gap formation for Tin Halide Perovskites.

In addition, tin oxidation is also attributed to the different band structures of lead-based and tin-based perovskites.

The minimum of conduction (CBM) is mainly made up of the p-orbital of a metal atom, while the maximum of the valence band (VBM) is composed of antibonding of p-orbital of halogen atoms and s-orbital of metal atoms. Considering the higher energy of the Sn 5s orbital than the Pb 6s orbital, the Sn-I bond is easier to break than the Pb-I bond *[17]*.

Theoretically, tin-based perovskites possess considerable better photo-electric properties than lead-based ones, with their suitable band gap (1.35 eV, 1.45 eV) for single junction solar cells close to the Shockley-Queisser (SQ) limit, smaller exciton binding energy, and higher charge-carrier mobility *[18]*. Perovskite materials can be formed with a large variety of cations and anions and even with mixture of them.

This allows to obtain material with a broad variety of bandgaps from 1.3eV up to 1.75eV (Figure 7) for mono-cation tin perovskite. When instead a mixture of cation is used the band gap could be further increase or decrease, this make perovskite suitable for many different applications also outside the photovoltaic world like OLEDs, tandem solar cells, scintillators and detectors or lasers *[19]*.

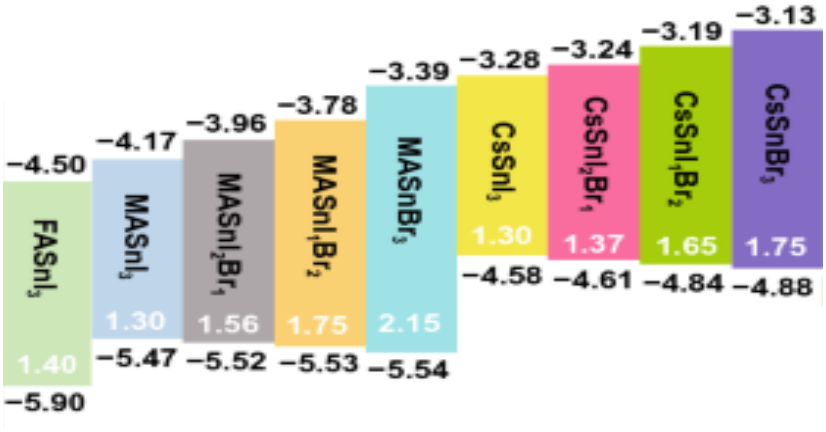

Figure 7 – Possible Tin Halide Perovskite composition and relative Bang Gaps.

1.3. Perovskite solar cell architecture.

Perovskite solar cells (PSCs), with active material of $FASnI_3$, $MASnI_3$ or $CsSnI_3$, typically have a planar structure where the perovskite active layer is sandwiched between a hole transport layer (HTL) and an electron transport layer (ETL). Two main types of device architecture for TPSCs, including *n-i-p* and *p-i-n* structures have been studied so far. Both device structures consist in two electrodes and three functional layers as show in Figure 8.

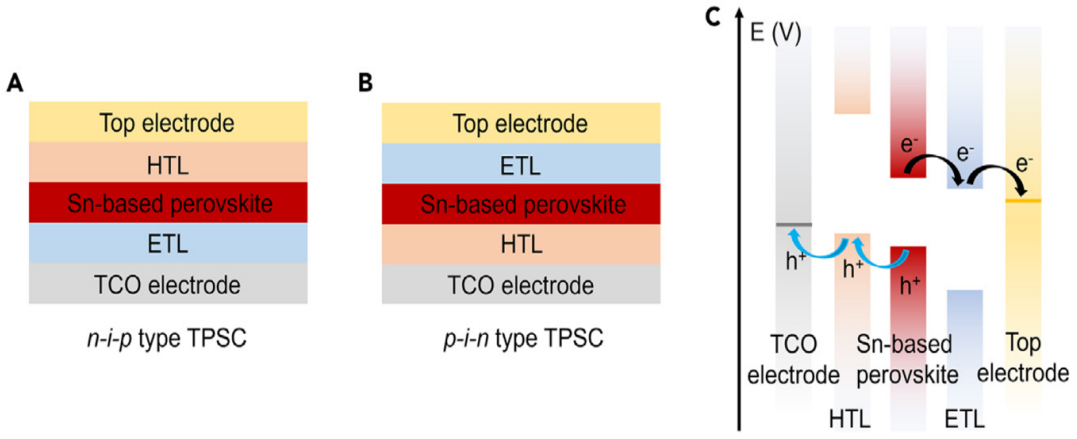

Figure 8 – Solar cell architecture and separation of changes scheme.

Up to date, in THPs solar cells the performance of the *n-i-p-type* TPSCs is much lower than that of the *p-i-n-type* TPSCs *[20]*.

Analyzing the *p-i-n* structure from bottom to top we have a transparent conductive electrode (TCO electrode) that is typically a glass coated with a conductive oxide (ITO). On top of it the function of the "hole transport layer" is to facilitate efficient hole carrier extraction and transportation from the perovskite layer to the transparent conductive electrode. Because in the inverted TPSCs light enters the devices from the HTL and coated TCO electrode side, the HTLs must be transparent enough to avoid light loss [21].

Nowadays, poly (3,4-ethylenedioxythiophene) – poly (styrene-sulfonate) (PEDOT:PSS) is the most promising solution since high efficiency cell can be obtained. PEDOT:PSS is a commercialized transparent conductive polymer with outstanding properties such as excellent conductivity, high transmittance, low-temperature annealing process and good flexibility make it suitable also for future flexible device *[22]*. This layer is deposited through solution process, since PEDOT:PSS is dispersible in water, on top of the transparent conductive electrode. On top of it the perovskite film, the active and absorber layer of the cell, is deposited. Immediately above it, the "electron transport layer" is deposited, which is typically fullerenes or their derivatives such as buckminsterfullerene (C60). The function of the ETL is to facilitate efficient electron collection and transport from the perovskite layer to the top electrode *[23]*. In conclusion a metal electrode deposited by thermal evaporations is apply, up to date gold and silver are the most utilized one *[24]*.

1.4. PSCs future challenges.

Tremendous efforts to tailor the optical and electronic properties of halide perovskites in terms of manipulating their grains size, surface, and component is currently done. Importantly, the growing potential of halide perovskite for advancing optoelectronic applications go beyond the only photovoltaic application including light-emitting devices (LEDs), scintillators, X-ray imaging,

lasers, thin-film transistors (TFTs), artificial synapses, and light communications *[9]*.

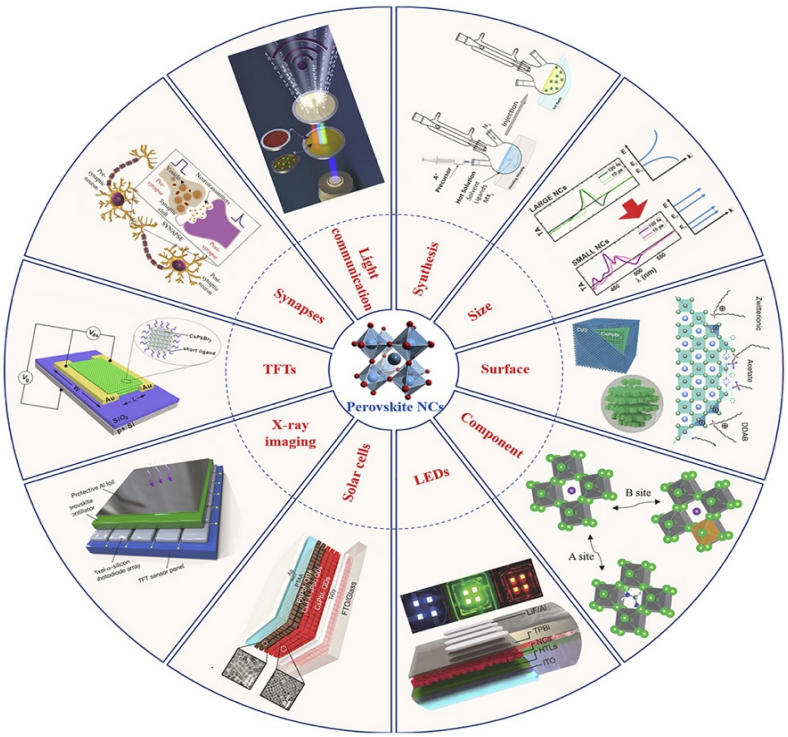

Figure 9 – Possible applications of Perovskite.

The typical lead-based organo-halide perovskite cells still pose challenges to commercialization, first of all due to the widely reported toxicity of lead with a negative impacts on plant growth, human and animal health, and the entire ecosystem. Moreover, natural reservoir of this material will be depleted quickly if a worldwide commercialization will occur.

Thus, lead-free perovskites are becoming popular for field applications in SCs. For Sn-based PSCs, the poor film quality and poor stability, the oxidation of Sn^{2+} to Sn^{4+}, are the two key challenges. Many efforts like modifying the synthesis method and use of additives have been carried out *[12][25].* Theoretically, THPs can outcome the efficiency of lead thanks to the narrow band gap close to the ideal one for single junction SCs but nowadays extra effort need to be done to understand the carrier transport dynamics and crystallization mechanism *[26]*.

Scientists are also looking for new materials that can offer better stability and novel properties against oxygen and humidity degradation increasing the life time of the devices.

1.5 Thesis objective

The purpose of this thesis is to understand the effects that each different monovalent cation (FA^+, MA^+, Cs^+), utilized in the perovskite structure, has on the morphology of the film, the crystallization process, and finally on the optoelectronic properties. This study aims to identify the optimal processing conditions for each cation type, leading to improved perovskite film quality and device performance.

2. Materials and Methods.

In this section the attention will be focused on the multiple steps required to produce a thin film of tin-halide perovskite with spin-coating techniques, highlighting for each of them the materials and the different approaches utilized. In addition a quick explanation on the working principles of the different characterization techniques utilized for the purpose of this work will be add.

2.1. Substrate preparation.

The substrate preparation depends on the subsequent studies that need to be performed. Hall Effect measurements and the fabrication of solar cells require an additional preparation step with respect to the other techniques because they necessarily use etched substrates, while the rest, such as XRD, SEM, Uv-Vis, and Four-points probe require only to cut Glass or ITO substrates in the right dimension to fit the instrument.

- ***Etching of the substrate.***

To create the final solar cells ITO-coated glass are needed to be etched to create two separate electrodes. The etching process utilized Zn powder and HCl 2M in H_2O, after an appropriate masking with tape of the substrate to remove the unwanted part of ITO. The substrate utilized for the Hall Effect measurements undergoes the same procedure changing the part of ITO removed as show in Figure 18. More often, to simplify the job, the substrates for the preparation of the cells were bought already etched from Ossila with two different dimensions of 2.8 x 2.8 cm and 2.5 x 2.5 cm.

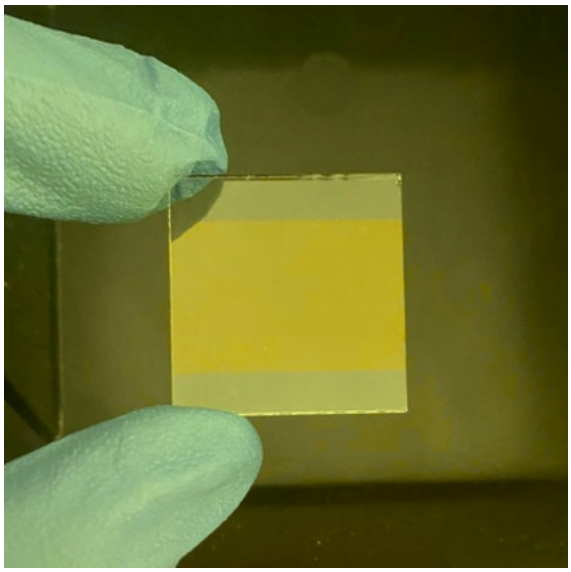

Figure 10 – Example of etched substrate for the preparation of solar cells.

- ***Cleaning of the substrate.***

The substrates were cleaned immediately before the deposition in a sonicator bath in soapy water, water, then acetone and finally isopropyl alcohol (IPA) for 15 mins each. The substrates were then dried with nitrogen from the residual IPA and treated within an oxygen plasma for 10 minutes to increase the wettability of the Glass and ITO coated glass substrates. This made easier to spread the precursor solution onto the substrates before the spin coating.

All the different substrates independently the final scope were treated in this same way. Etching and cleaning of the substrates are performed in air, while

the rest of the deposition occurs in nitrogen-filled gloveboxes, where low ppm of oxygen and humidity are ensured (<0.5 ppm).

2.2. Hole-selective layer deposition.

As mention at the beginning in the PSCs architecture paragraph, to be able to work properly a hole selective layer is needed in between the ITO surface and the perovskite layer.

The PEDOT precursor was made diluting 200μl of PEDOT with 800μl of toluene. The solution was dripped during the first 5 seconds of the spin coated at 500 rpm, then after the first five seconds the velocity was raised to 4000 rpm for 25 more seconds. At the end of the spin coating a thermal annealing was perform at 150°C for 10 minutes.

The Al_2O_3 instead was then diluted 1:100 (vol : vol) utilizing 20μl of Al_2O_3 and 1000μl of isopropyl alcohol (IPA) and then spin coated over the annealed PEDOT following the same procedure as before.

The thermal annealing for this layer was done at 100°C for just 3 minutes, the time needed to make the IPA evaporate and leave only the Al_2O_3 particles.

2.3. Tin-halide solution preparation.

The pristine $ASnI_3$ perovskite films were prepared utilizing A= FA^+, Cs^+ and MA^+, in combination with slightly different deposition parameters to achieve the best film quality possible for each cations.

CsI (99.999%), SnI_2 (99.99%), dimethylformamide (DMF), dimethyl sulfoxide (DMSO), and chlorobenzene were purchased from Sigma-Aldrich.

MAI and FAI were purchased from Great cell Solar instead.

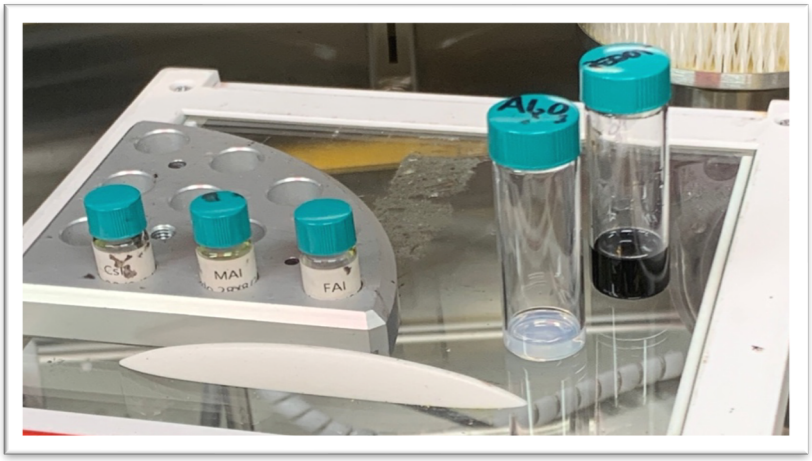

Figure 11 – Prepared Perovskite precursors solution (left) and PEDOT:Al_2O_3 (right).

A stock solution for the three cations were prepared with a molar ratio of 1:1 mixing FAI, MAI and CsI powders with a SnI_2 precursor. Then DMF/DMSO mixed solved (4:1 v/v) were added to obtain 1.2 M solution. The vials were then stirred on the hot plate for 30/35 minutes and a yellowish solution was obtained.

2.4. Spin-coating process

Figure 12 – View of the glovebox and spin coater details.

Thin films were deposited inside a nitrogen filled glovebox. The spin coater was a Laurell WS-650-23B that has a chamber with a rotatory holders that kept the substrate steady thanks to a small vacuum pump.

The deposition process can be divided in 3 steps:

i) Spin coating setting : Where precursor solution was dripped and the spin coater parameters were set.
ii) Quenching of the precursor: an essential step to remove the excess of solvent DMF:DMSO. This is typically done to improve the film quality and the perovskite crystal formation and can be achieved with different techniques.
iii) Annealing of the film: This is performed typically to improve the grains size inside the film thanks to the supply of energy that is provided from this step.

2.5. Thermal evaporation.

Thermal evaporation has been used to deposit the electron transport layer and top metal contact on top of the perovskite thin film to fabricate solar cell devices. The PEDOT/PVSK stacks were first scratched to remove the perovskite where the back silver contacts need to be in contact with the ITO-coated glass substrate, then they were put in place inside a metal mask that was used to obtain the final shape of the pixel that needed to be tested and also to made them steady during the evaporation process. The mask was placed inside the metal evaporator into a rotatory holder that helped to achieve a better and homogeneous deposition.
In Figure 13 a chamber view show on the left the two holders for the organic components (C60, BCP) that were heated up by a resistance coil, while on the right a "boat" was attached to two electrodes making possible to evaporate metal (Ag, Au …) through flowing an electric current in between them. For the deposition to occur a high vacuum up to $1*10^{-7}$ mbar was required.

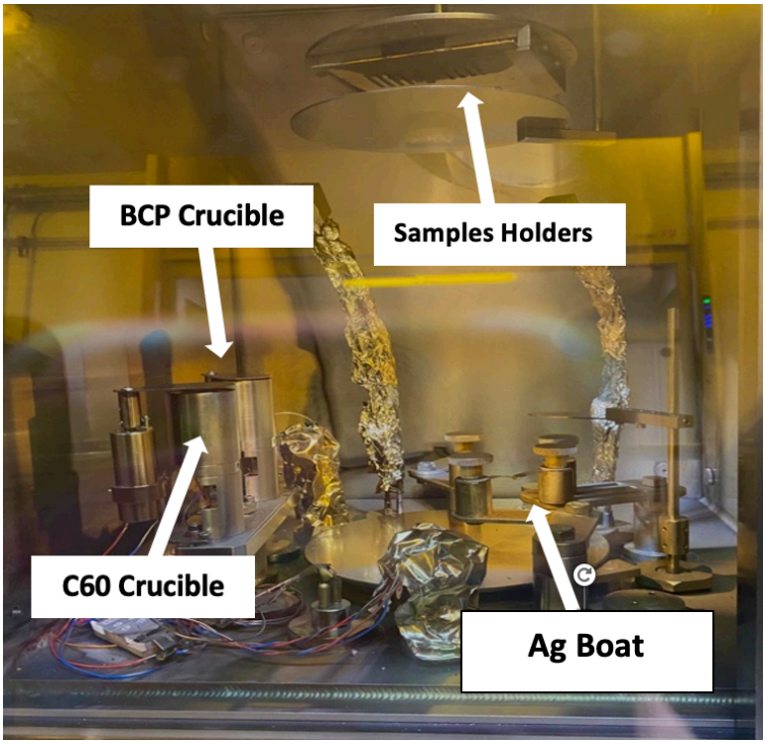

Figure 13 – Evaporator chamber internal view

- ***Electrons transport Layer (C60).***

The electron transport layer of C60 was evaporated onto the perovskite with a thickness of 25 nm. The evaporation rate was kept constant at 0.1 Å/s for the first 10 nm of the evaporation to allow a slow and smoot adhesion of it, creating less defect at the interface. Then, the evaporation rate was increased at 0.3 Å/s till the conclusion of the process. The temperature was set at 400°C to initialize the evaporation procedure, than little adjustment were perform to kept a constant rate.

- ***BCP Buffer Layer.***

Bathocuproine (BCP) is a commonly used buffer layer and is thermally evaporated after the C60 with a thickness of 3nm with a deposition rate of 0.1 Å/s. It has been demonstrated that the buffer layer at the interface between the ETL and metal electrode in the inverted TPSCs are pivotal to achieve efficient devices. The buffer layer not only reduces the Schottky barrier between the ETL

and metal electrode due to the tendency of this layer to chelate with metal electrodes but also prevents the corrosive problems caused by moisture in ambient and ion diffusion *[24]*.

- ***Ag contacts***

The back contacts were then evaporated on top of the all stack to complete the cells. Silver was utilized because higher performances can be achieve compare to when gold is the material that compose the contacts. The boat containing Ag pellets was heated up and a 125 nm layer was deposited with a rate ranging from 0.1 to 0.7 Å/s.

2.6. Encapsulation of the Samples.

The encapsulation step was required when the samples needed to be taken outside the nitrogen-filled glovebox to avoid oxidation and degradation of the material. Typically this was done for measurement such as Uv-Vis, Hall Effect and for testing the cells in the Solar Simulator. In this work we have used glass to glass encapsulation using ultraviolet (UV) light curable epoxy edge sealant. The glue was purchased from Everlight Chemicals. When the glue was settled down a Uv-lamp was used for 50 sec to hardening it.

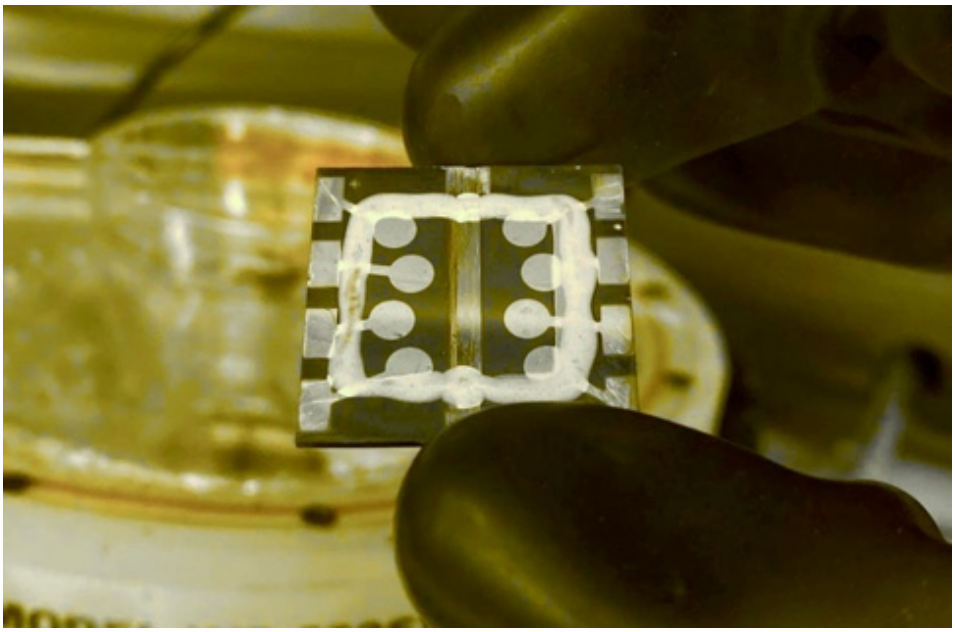

Figure 14 – Final result of a finish cell after encapsulation.

3. Characterisation Techniques.

- ***UV-Vis-NIR Spectroscopy.***

This spectroscopy techniques analyses the absorption of the tested material in the ultraviolet (UV), visible (Vis) and near infrared (NIR) regions of the electromagnetic spectrum. The measurements on perovskites were performed with the PerkinElmer LAMBDA 1050+ within a 450-1100nm wavelength range after the encapsulation of the samples to preserve their crystalline structure and properties. From the absorption curve that was obtained same parameters can be extrapolated. Through different approaches for example the Tauc Plot, important correlation with the band gap of the tested materials can be evaluate. The band gap could also be extrapolated from Photoluminescence (PL) measurement, from the maximum of photoluminescence emission through conversion in eV.

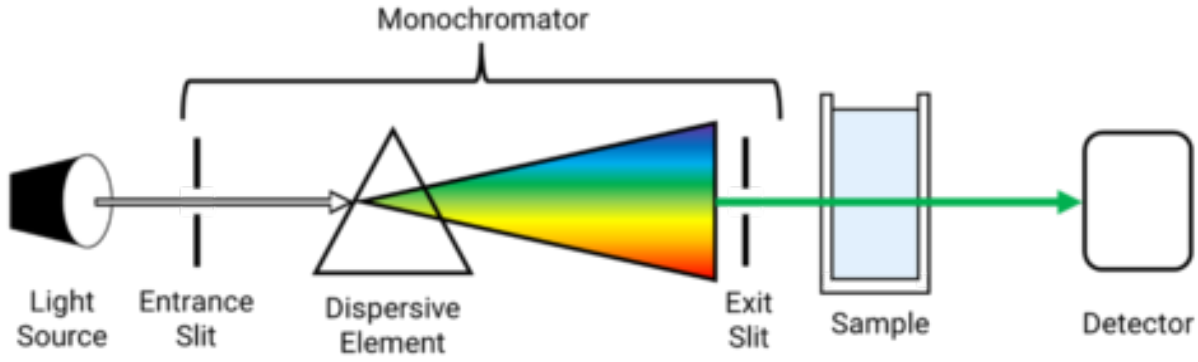

Figure 15 - Uv-Vis working principals scheme.

- ***X-Ray Diffraction (XRD)***

X-ray diffraction (XRD) is an indispensable tool for characterizing thin films of perovskite materials and the working principals are quite easy to understand. An incoming X-rays beam is diffracted by the regular structure of the crystal whit a specific angles and intensities. For this work a BunkerD8 Advance with a Bragg-Brentano geometry was utilized, show in Figure 16 and the X-ray in this specific model are generated by a copper anode with a specific wavelength of

1.541 Å. The X-rays excite the electrons present in the crystal that become secondary sources. The electromagnetic waves produce by those e^- interact constructively only along certain directions depending on the crystal structure and crystal planes, while they cancel each other out over the other directions. Scanning the area around the sample with a rotating detector gives the ability to determine specific characteristics of the material, this technique is called Theta - 2Theta Scan, where Theta, the incident angle of the X-ray beam, is kept constant at a certain value typically below 5° to minimize the penetration in the film of the incoming X-ray, while 2Theta, the detector intended to capture the reflected X-ray, is set to move from one angle to another in order to capture al the signal in that range. In this work, 2Theta was ranged from 10° to 60° for Tin perovskite thin films *[27]*.

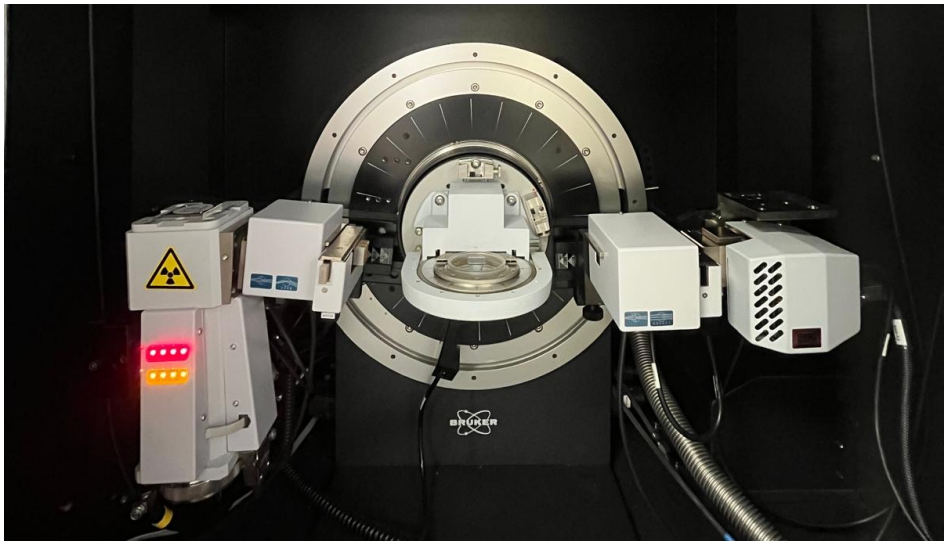

Figure 16 – View of XRD, X-ray beam(right), sample holder (center) and 2-theta detector (right).

- ***Scanning Electron Microscope (SEM).***

A scanning electron microscope is type of electronic microscope that produces images of the samples by scanning the surface with a focused beam of electron. The electrons interact with atoms in the sample, producing various signals that contain information about the surface topography and composition of the sample. In the most common SEM mode, secondary electrons emitted by atoms excited by the electron beam are detected using a secondary electron

detector. Some SEMs can achieve resolutions better than 1 nm when analyzing the samples under high vacuum condition.

For the purpose of this work a Tescan Mira$_3$ FEG-SEM was used. Scanning electron microscope (SEM) pictures are useful for examining the fine structure and the grains arrangement of the perovskite layer providing a powerful technique to analyze the morphology and the cross-sections derived from different deposition methods.

- ***4-Point Probes.***

Sheet resistance (also known as surface resistance or surface resistivity) is a common electrical property used to characterize thin films of conducting and semiconducting materials. This property can easily be measured using a four-point probe and is critical in the creation of high-efficiency perovskite photovoltaic devices, where low sheet resistance materials are needed to extract charge.

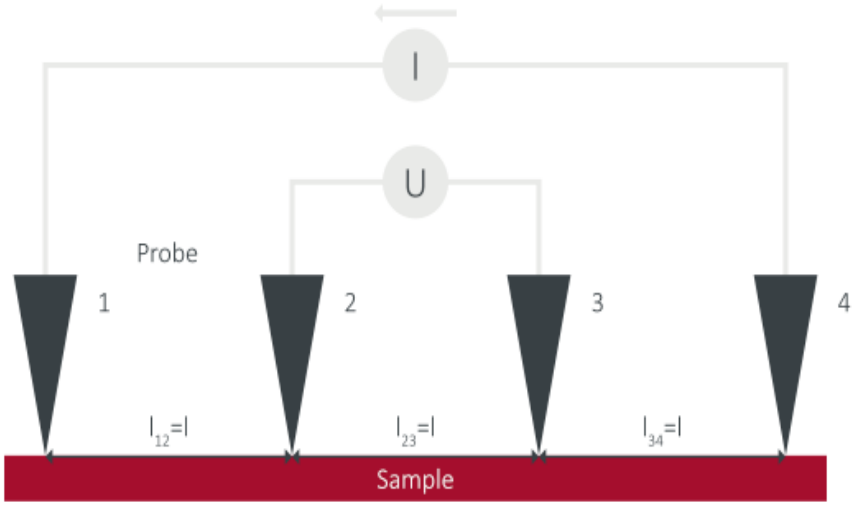

Figure 17 – 4-point probe working scheme.

The primary technique for measuring sheet resistance is the four-probe method (also known as the Kelvin technique), which consists of four equally spaced, co-linear electrical probes, as shown in picture. It operates by applying a current (I) between the outer two probes and measuring the resultant voltage drop between the inner two probes as show in Figure 17.

Furthermore, the resistivity and conductivity can be calculated if the sheet resistance and material thickness are known through Eq. 4.

$$\boldsymbol{Conductivity(S/m)} = \frac{1}{\boldsymbol{Sheet\ Resistance\ (Ohm/sq)} \times \textbf{Layer thickness (nm)}} \quad (4)$$

This allows for the materials to be electrically characterized, purely by taking a sheet resistance measurement.

- ***Hall Effect.***

The Hall effect is a valuable tool for characterizing tin perovskites. By measuring the Hall voltage, it is possible to determine the carriers concentration and mobility of these material, which are important parameters for understanding their properties and optimizing their performance in various applications. For tin halide perovskites, the Hall effect can be used to measure the carrier concentration (number of charge carriers per unit volume) and mobility (how easily charge carriers move through the material). By applying a magnetic field to the film and measuring the Hall voltage, it is possible to determine these important properties. To conduct the Hall effect measurement a suitable substrate need to be use. As show in Figure 18 the ITO-coated glass need to be etched (Etching of the substrate) leaving four squares of it at the corner of the samples. After the spin coating and the annealing the excess of perovskite was removed leaving an inner single square in contact with the all for ITO parts. Before the measurement an encapsulation process was carried out to protect the sample from air exposition.

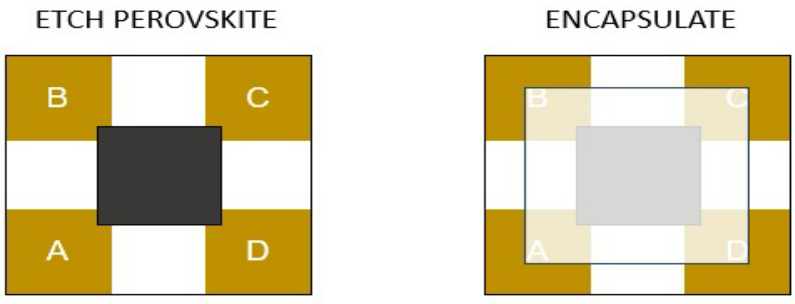

Figure 18 – Example of substrate preparation for Hall Effect measurement.

- ***Current-Voltage curve.***

To characterize the solar cells, a Solar Simulator is typically utilized to extrapolate the JV curve of the cells that give us important parameters. A Newport Oriel Sol3A solar simulator was used with a light intensity of 1 Sun that mimicking the solar spectrum at the earth surface for a valid comparison with the real working environment.

From the JV curve important parameters can be extrapolated: the *short circuit current* (J_{SC}) is evaluated when the voltage across the device is null; on the other end; the *open circuit voltage* (V_{OC}) is defined as the voltage at which the current flowing in the solar cells is zero. The Fill Factor (*FF*) represents the squareness of the IV curve and can be evaluated knowing the maximum power, *Jsc* and *Voc* (equation 5). The Power Conversion Efficiency (PCE) of the solar cell is a critical metric in the development and comparison of different type of solar cells. It measures of how effectively a solar cell converts sunlight into usable electrical energy, it is expressed as a percentage and is calculated using equation 6.

$$\boldsymbol{FF = \frac{PMax}{Jsc \times Voc}} \qquad (5)$$

$$\boldsymbol{PCE(\%) = \frac{Output\ Power\ (Electric)}{Input\ Power\ (Light)} = \frac{Jsc \times Voc \times FF}{Plight} \times 100} \qquad (6)$$

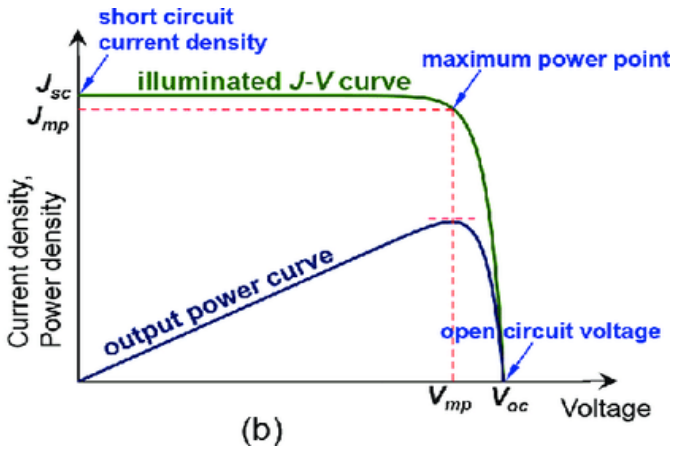

Figure 19 – Typical current-voltage curve with highlights of the points of major interest.

4. Results and discussion

This chapter shows more in detail the procedures and the steps needed to prepare and optimize the different perovskite films explaining the possible reasons and interpretation for the results obtained..

4.1. Previous work.

The starting point for this thesis was set thanks to previous work carried out within the Italian Institute of Technology (IIT), which aimed at using Sn halide perovskites for thermoelectric applications. Preliminary data found that Sn based perovskites prepared with different cations exhibited considerably different morphologies and electronic properties, as suggested by the SEM top view images shown in Figure 20. These films were obtained starting from a precursor solution prepared by adding 1:1 mixture of SnI_2 with the respective organic or inorganic cation. The mixture was then dissolved in DMF and DMSO with a 4:1 ratio for a total concentration of 1.2 M. Films were spin coated at 1000 rpm for 10 s and 4000 rpm for 30 s in a nitrogen filled glovebox.
Chlorobenzene was dripped on to the spinning substrate after the first 18 s of

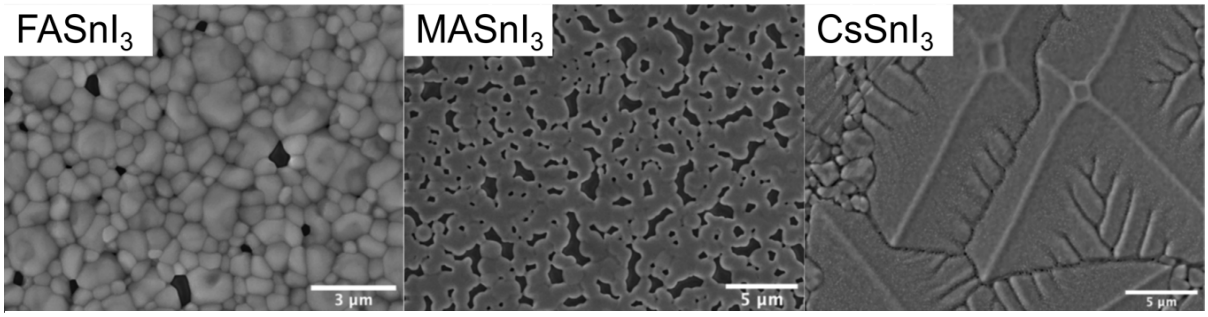

Figure 20 – SEM top view of reference films.

the spin-coating process. The spin-coated films were annealed at 50 °C for 20 minutes and then at 100 °C for 20 minutes giving the film shown in Figure 20.
The characterization of the obtained film displayed a band gap for $FASnI_3$, $MASnI_3$, and $CsSnI_3$ of 1.42, 1.3, and 1.33 eV, respectively. The three single-cation perovskites $FASnI_3$, $MASnI_3$, and $CsSnI_3$ showed room-temperature electrical σ values of 5.7, 23.5, and 99.4 S cm^{-1} *[28]*.

From these results the aim of this thesis project was to further increase the film morphology, reducing pinholes and improving film coverage, through deposition engineering. So to set the goal of this project a few questions were posed.
Is it possible to further optimize the film morphology reducing the pin holes and what are the main deposition techniques to do it? Is there any correlation between the morphological properties of each Sn perovskite films and their different electronic proprieties?

4.2. Deposition settings

The three phases of the spin coating process were changed to optimize the films quality:

i) Spin coating setting
ii) Quenching step
iii) Annealing step

▪ *Spin coating setting*

The rotation speed of the spin coater is an important parameter the allow for a formation of homogeneous and thick films. Starting from the previous work the settings have been changed to understand the effect on the final product.
Two different setting were carried out, trying to understand the effect on the film morphology with further characterization.

SPIN COATING SETTING tested:

1 *4000 RPM for 50 seconds*

2 *1000 RPM for 10 seconds and 4000 RPM for 50 seconds*

- ***Quenching step***

Anti-solvent quenching:

Many methods and treatments have been introduced to optimize the product quality by improving the surface homogeneity and crystallinity of the films and the utilization of antisolvent is one of the most utilize *[29]*.

The antisolvent, in our case, was used to evaporate the DMF:DMSO mixture during the spin coating process. The antisolvent doesn't have to react with the precursor of the perovskite solution. When it is apply local regions of supersaturation are created due to solvent evaporation, accelerating heterogeneous nucleation. It is believed that an intermediate phase between antisolvent and perovskite precursor is formed slowing down the crystallization. This phenomena has a strong effect in Pb-PSs but is it less intense for Tin perovskite *[30]*.

The antisolvent utilized in this thesis work were: Anisole for $FASnI_3$ films and Chlorobenzene for $MASnI_3$ and $CsSnI_3$ films.

Gas quenching:

The gas quenching technique doesn't rely on antisolvent and is a valid alternative that can also offer a cleaner process when looking at environmental concerns.

During the spin coating, after a certain time, a stream of N_2 gas was directed on the substrate and left there till the end of the process to evaporate the DMF:DMSO solvent and form the thin film of perovskite *[31]*.

QUENCHING TECHNIQUES tested:

1 *Not use of antisolvent nor gas quenching*

2 *Antisolvent after 25 seconds*

3 *Antisolvent after 45 seconds*

4 *Hot Antisolvent at 65°C*

5 *Gas quenching for 25 seconds*

- ***Thermal Annealing.***

In the formation of high quality film annealing is the most crucial part and in the past years several different techniques were studied for example pressure annealing, electromagnetic waves annealing, physical annealing and ultrasonic annealing.

Among all the options above the most valuable and the most common remain the thermal annealing that consists in heating up the substrate after the spin coating on an hot plate. This step is required to completely remove the organic solvent and crystallize the perovskite film and to provide energy to the crystal growth phase. The time and temperature of the thermal annealing determines the quality of the crystals *[10]*.

The choice of the "annealing window" can be made in function of the time or the temperature depending on the interests and the application. Annealing at higher temperature could induce the faster removal of the solvent to create a supersaturation condition, which would accelerate the nucleation and create an higher density of nuclei in the film. On the other hand annealing with a lower temperature can be exploited in certain case or for environmental prospective but the prolonged time usually needed may lead to problem with film and device stability due to the fragility of the tin perovskite structure *[32]*. Gradient thermal annealing was also found to have positive effect on the films morphology slowing down the evaporation rate of the solvent and slow down the crystallization of the films.

For the purpose of this work after optimization of the first two steps of the spin coating the annealing temperature was modify as follow to understand its effects.

ANNEALING PARAMENTERS tested:

1 *100°C for 20 minutes*

2 *120°C for 20 minutes*

3 *150°C for 20 minutes*

4	*5 minutes Ambient temperature plus 15 minutes at 100°C*
5	*10 minutes Ambient temperature plus 10 minutes at 100°C*
6	*15 minutes Ambient temperature plus 5 minutes at 100°C*
7	*40°C for 20 minutes plus 80° for 20 minutes*
8	*Slow increase from 40°C to 100°C → (5°C every 90 seconds)*

4.3. $FASnI_3$ film optimisation

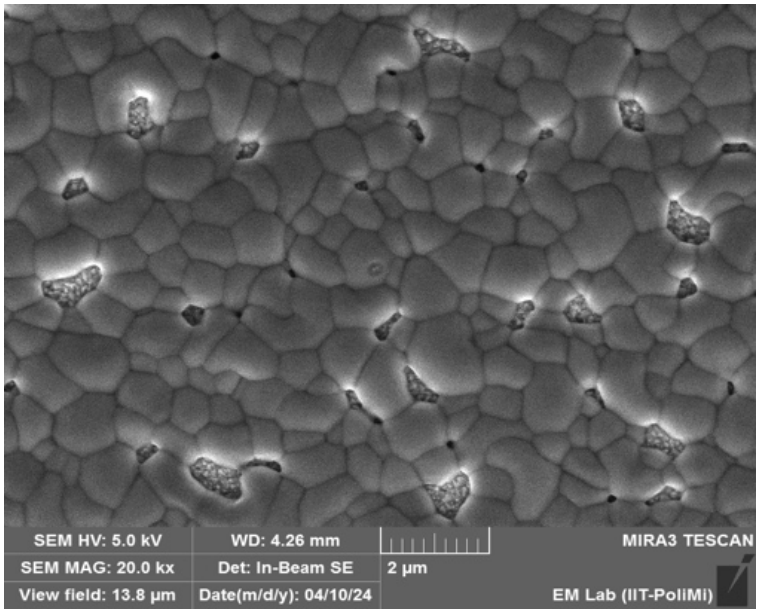

Figure 21 – SEM top view for FASnI3 Film 1F

The Figure 21 above shows the FASnI3 film achieved with a spin coating at 4000 rpm for 50 seconds and an anisole dripping after 25 seconds (referred to as *Film 1F)*. Subsequentially a thermal annealing at 100°C for 20 minutes was performed as suggested from previous work. The film structure show sign of large pin holes leaving expose the bare ITO substrate below. This could lead to leak in current due to the possible contact between hole transport and electron transport layers.

The formation of the pin holes is believed to be mainly due to the shrinkage of the perovskite structure after the antisolvent dripping. To optimize the quality of the film the parameters that have been changed are listed above in Deposition settings. *A second attempt of optimization for FASnI3 was carried out (referred*

to as Film 2F) the film was obtained from pristine solution utilizing the same spin coating setting as *Film 1F* changing instead the annealing temperature. In this case a slow ramp-up from 40°C up to 100°C was performed rising the temperature by 5°C every 90 seconds. The film obtained showed a strange morphology of the grains that did not achieve a round shape, a clear sign of uncomplete formation. The reason to this accordingly to existing literature is that a lower energy is provided at the beginning of the crystallization process enhancing the nucleation phase instead that the grow phase of the forming crystal *[33]*. The crystallization for THP tin Halide Perovskite is typically faster than in LHP Lead Halide Perovskite, this is one of the main reason of the poor morphology of the films. To enhance it energy needs to be provide through the thermal annealing process but the rapid evaporation of the remaining solvent and antisolvent inside the perovskite could lead to cracks and pin holes formation. Due to this reason a third film (referred as to *Film 3)* was obtained with a technique called “ageing” ,this consist in left the deposited film at room temperature for 5 minutes before being thermal annealed for 15 minutes on the hot plate at 100°C.

The idea was to have a first step for slow crystallization without supply of energy follow by a thermal annealing to enlarge the already formed nucleation centers, the results show lots of nucleation centers that gave in the end a film with less pin hole than the previous two but where the average grains size were still small and without a define form. In the end another strategy that has been explored to improve the coverage was to change the spin coating setting. Instead of starting the process immediately with 4000 rpm, ten second were added at the beginning with a rotational speed of 1000 rpm for the preparation of another film (referred to as *Film 4F*). This new spin coater settings were tried with the already tested different annealing temperatures and among all of them the best result was achieved with an annealing at 100°C after the deposition. The final *Film 4F* had a full coverage among all the substrate without pin holes and with few bigger grains respect to the previous samples. The initial slower rotational speed could probably be responsible for the homogeneity of the coverage, this

probably gave time to the solution to spread slower and with a better uniformity on the substrate at the beginning of the spin coating. The higher temperature provided could have led to a slower crystallization with a further growth for some grain seed.

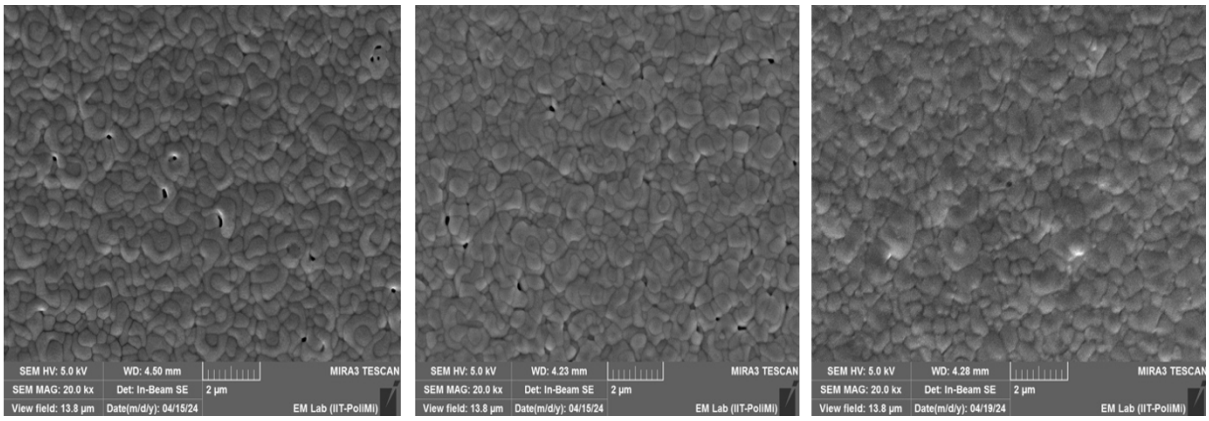

Figure 22 – $FASnI_3$ samples SEM top view for Film 2F (left), Film 3F (center), Film 4F (left)

To gain further insight into the morphology and thickness of the fabricated layers, cross-sectional images of the samples were acquired using Scanning Electron Microscopy (SEM).

While the properties of perovskite films are typically assessed in the horizontal plane; for instance, conductivity measurements are influenced by the presence of grain boundaries and defects within the film, in photovoltaic devices, the vertical transport of charge carriers is paramount. This is because the collection of electrons and holes, generated upon the absorption of light energy, is facilitated by the Electron Transport Layer (ETL) and Hole Transport Layer (HTL), which are positioned above and below the perovskite film, respectively. Consequently, it is crucial to investigate the cross-sectional structure of these thin films, in addition to their top-view morphology, to gain a comprehensive understanding of their suitability for photovoltaic applications.

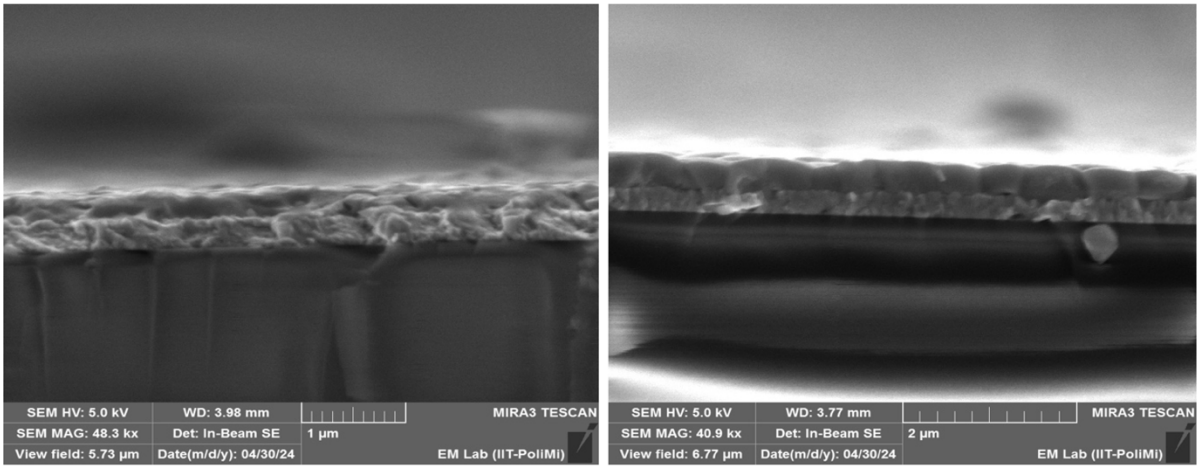

Figure 23 – SEM Cross-section view for $FASn_3$ Film 3F (left) and Film 4F (right)

A particularly insightful comparison emerged from the analysis of *Film 3F* and *Film 4F*, which were fabricated using two different spin-coating parameters. As illustrated in Figure 24, *Film 4F* exhibits well-defined grains in both the lateral and longitudinal directions, with a uniform distribution throughout the cross-section. In contrast, while *Film 3F* also demonstrates a homogeneous structure, distinct grain boundaries are not readily identifiable in the SEM images. Furthermore, the vertical arrangement of the grains in *Film 3F* appears less well-defined. *Film 4F* exhibits a slightly greater thickness, which can likely be attributed to the slower initial spreading of the precursor solution on the ITO layer during the modified spin-coating process. These morphological differences, stemming from variations in the fabrication process, could have a direct impact on the performance of the respective films.

- ***XRD measurement***

The three films presented above were then characterized with XRD to assess the crystal structure of the perovskite. Theta was set at 3° to minimize the penetration of the X-ray beam inside the film. 2Theta was set to scan the deflected beam from 10° to 60°. Typical perovskite peaks for $FASnI_3$ are expected at around 14° 24° and 28° that correspond to the crystal planes 100, 111, 200 respectively, then the peak around 32° correspond to the 012 plane and the 40° peak account for the 022 plane.

The result show a orthorhombic structure with complete formation of perovskite with no residues of precursors, this can also be confirmed from literature *[34]*. In the end no variations of XRD scan among the 3 samples were observed meaning that the different approaches led to changes in the morphology structure but not in the arrangement of the crystal structure.

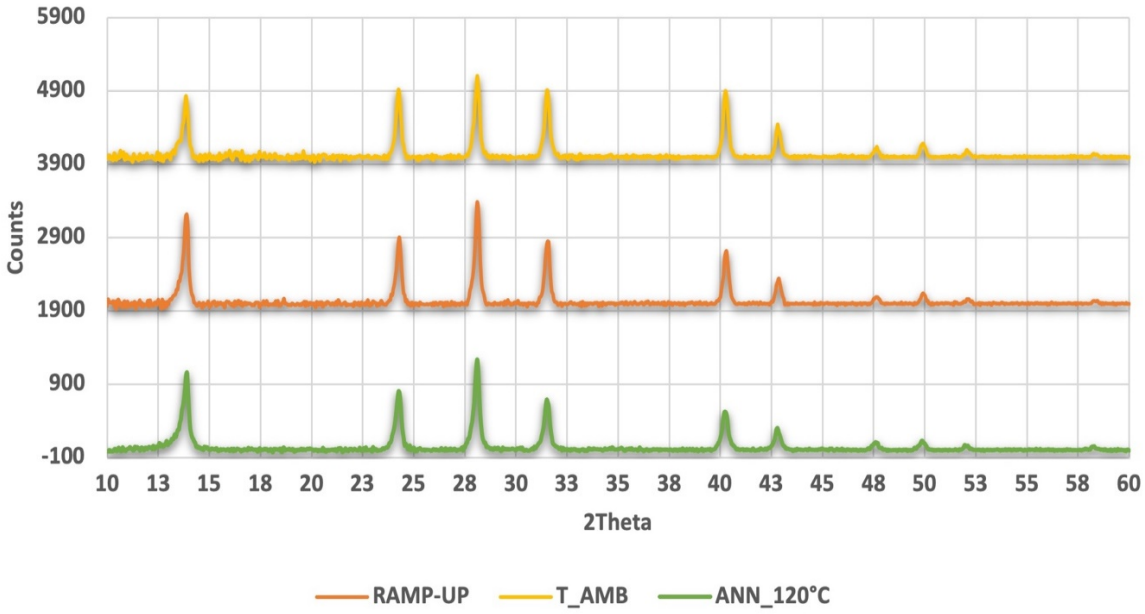

Chart 1 - XRD results for film $FASnI_3$ samples. Film 2F (middle), Film 3F (top) , Film 4F (bottom). 2-Theta scanning angles from 10° to 60

°

- ***Four-point probe and Conductivity***

The three selected film were then reproduced to characterize the sheet resistance and from it the conductivity. The measurement was perform within one hour from the end of the spin coating and annealing procedure inside the glovebox thanks to portable four-point probe. This was done to test fresh film and avoid degradation that can occur even if the film are stored in a N2 atmosphere. Below the results show that the conductivity of the films change from 0.53 S/cm for Film 2F to 4.08 S/cm for Film 4F.

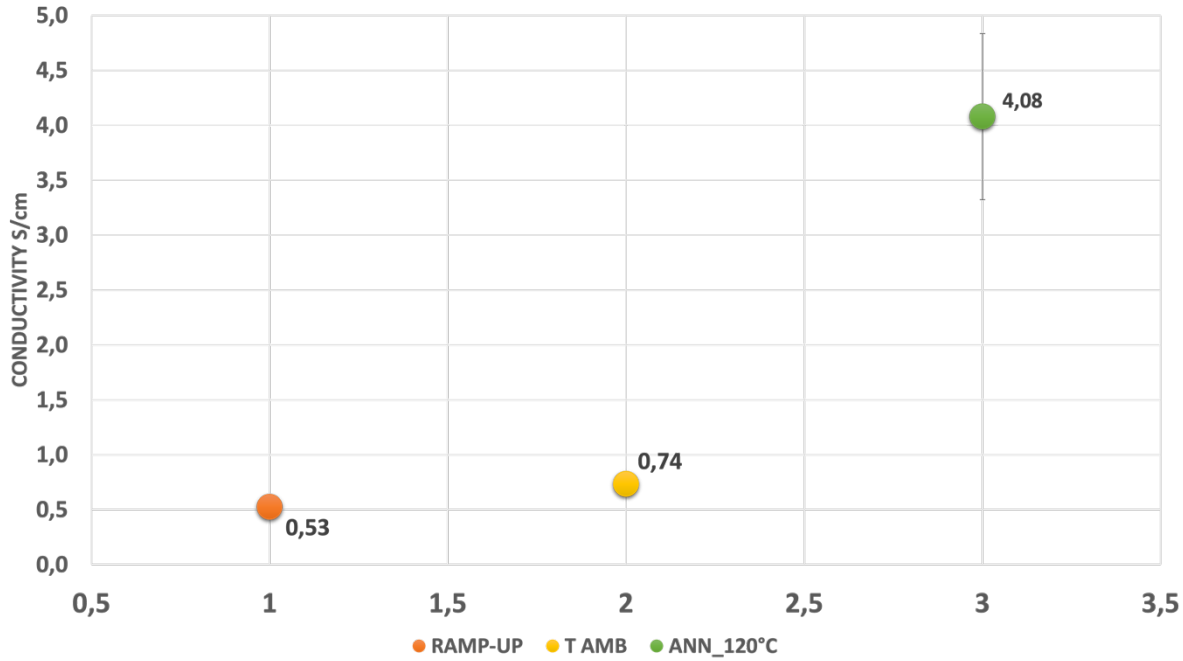

Chart 1 - Conductivity measurement with 4-Point Probe for Film 2F (left) Film 3F (center) Film 4F (right).

- ***Uv-Vis results***

The selected *Film 4F* that showed the better morphology was then tested to characterize the absorption profile in the range of wavelength between 400 – 1000 nm. From the results obtained the Band Gap was calculated, leading to a band gap value of 1.43 eV that is in line with the results found from previous work.

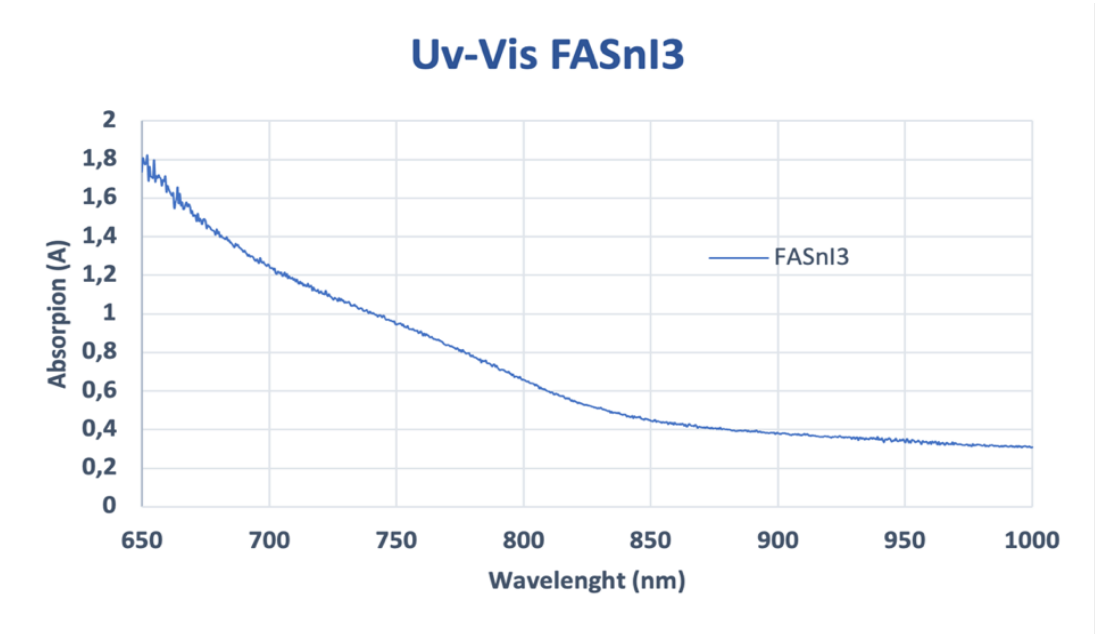

Chart 2 – Uv-Vis measurement for optimized Film 4F

4.4. $MASnI_3$ film optimisation

The optimization process for $MASnI_3$ films began with the spin-coating of a precursor solution, prepared by stirring the precursors in a 4:1 mixture of DMF and DMSO for 30 minutes at 35°C. This procedure was consistently followed throughout the study. Although the advancements made with $FASnI_3$ provided valuable insights, the intrinsic differences in the characteristics of each cation necessitated a distinct optimization approach for $MASnI_3$ films.

A difference in the $MASnI_3$ process was the use of chlorobenzene as the antisolvent, replacing anisole which had proven optimal for $FASnI_3$. The initial $MASnI_3$ film, designated as *Film 1M* (reference), was prepared using a spin-coating procedure with a rotation speed of 4000 rpm for 50 seconds and chlorobenzene dripping after 25 seconds into the process. Subsequently, the film underwent annealing at 100°C for 20 minutes. However, this film exhibited a significant presence of pinholes, a commonly reported issue in the literature for $MASnI_3$ *[13]*.

To address the pinhole problem, a technique involving a heated antisolvent was employed for the fabrication of *Film 2M* (hot CB).

Drawing inspiration from the successful results obtained with *Film 4F*, a two-step spin-coating procedure was implemented: 1000 rpm for 10 seconds followed by 4000 rpm for 40 seconds. The chlorobenzene antisolvent was heated to 65°C prior to being dripped onto the spinning substrate 25 seconds into the process. This hot antisolvent method is believed to promote crystal growth and enhance film quality. Indeed, as show in Figure 25, *Film 2M* exhibited significantly larger grain sizes, approximately three times the area compared to *Film 1M*. Despite this improvement, the presence of large pinholes remained an issue. The formation of these pinholes, as previously discussed, is primarily attributed to film shrinkage induced by the antisolvent, and the modified rotational speed alone was insufficient to overcome this challenge *[29]*. Further optimization with the investigation of gas quenching as a potential solution was carried out.

Film 3M (GQ) was fabricated using the N_2 gas quenching method. This involved applying a stream of nitrogen gas to the substrate for 25 seconds during the spin-coating process, followed by annealing at 120°C for 20 minutes. The nitrogen stream appeared to slow down the solvent evaporation process during spin-coating. The resultant Film 3M demonstrated uniform substrate coverage without any discernible pinholes, representing a significant improvement in film quality.

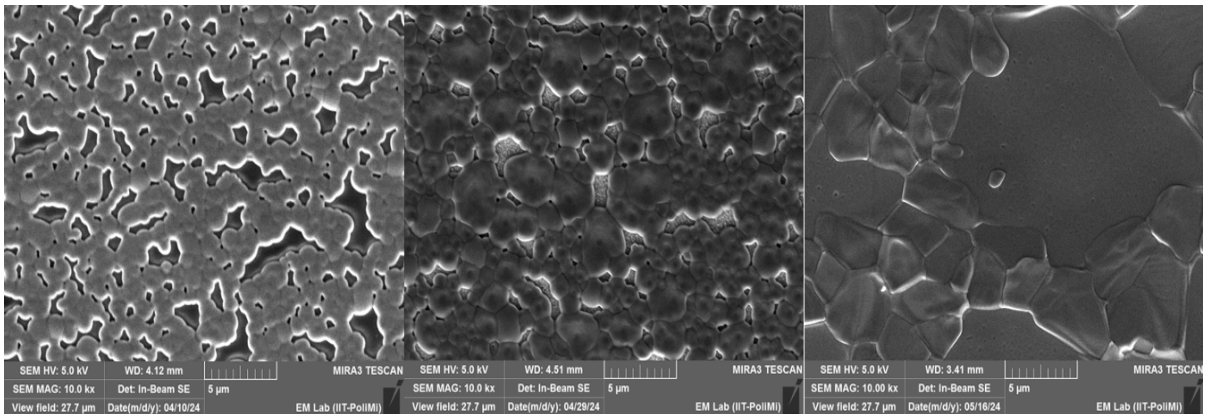

Figure 24 – $MASnI_3$ samples SEM top view for Film 1M (left), Film 2M (center), Film 3M (left).

- ***XRD measurement***

The three films characterized with the XRD present a crystalline structure with 100 plane and 200 planes peak with higher magnitude compere to $FASnI_3$ film. No peaks for residual precursor in the films were identified. MASnI3 film had overall higher crystallinity with respect to $FASnI_3$, which could be assigned to the better fit of MA^+ cations in the lattice of perovskite.

No distortions were observed among the three XRD of the films even though the SEM images differ in morphologies. An assessment of the intensity ratio between plane 100 and plane 200 was perform leading to results of 11.59, 6.62 and 14.29 for *Film 1M, Film 2M* and *Film 3M* respectively.

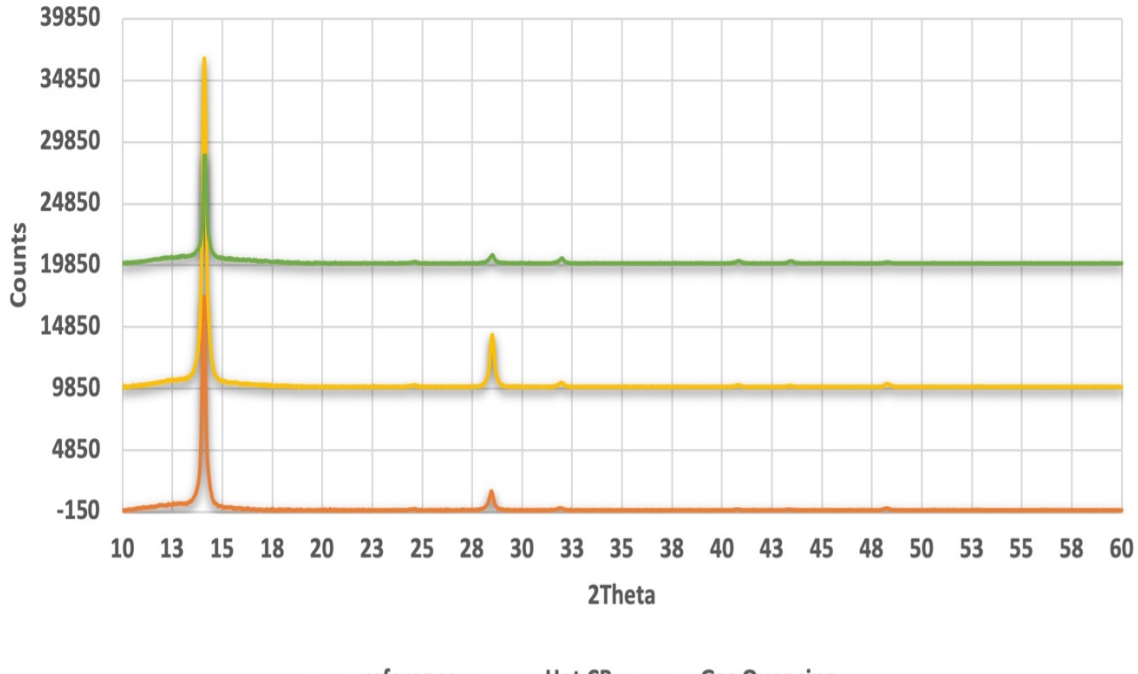

	2Theta 14.16°	2Theta 28.45°	ratio
Reference:	17485	1224	14,29
Hot CB:	53313	8057	6,62
Gas Quenching:	34439	2872	11,59

The film prepared with the gas quenching techniques show then a better orientation and growth of the crystal, this could led to a better mobility and diffusion length of the free charges

- ***Four-point probe and Conductivity***

The three selected films were then reproduced to characterize the sheet resistance and from it the conductivity. The measurement was performed within one hour from the end of the spin coating and annealing procedure inside the glovebox. This was done to test fresh film and avoid degradation that can occur even if the film are stored in a N_2 atmosphere. The result below show how the conductivity move from 11.79 S/cm for Film 1M, that presented small grain size and large pin holes, to 5.12 S/cm for Film 2M that still had pin holes but with enhanced grain dimension and in the end to a value of 3.33 S/cm for Film 3M that showed full coverage of the substrate.

Since no changing were observed in the XRD measurement one valuable reason could be reconduct to absence of pin holes and the homogeneous surface morphology and alignment.

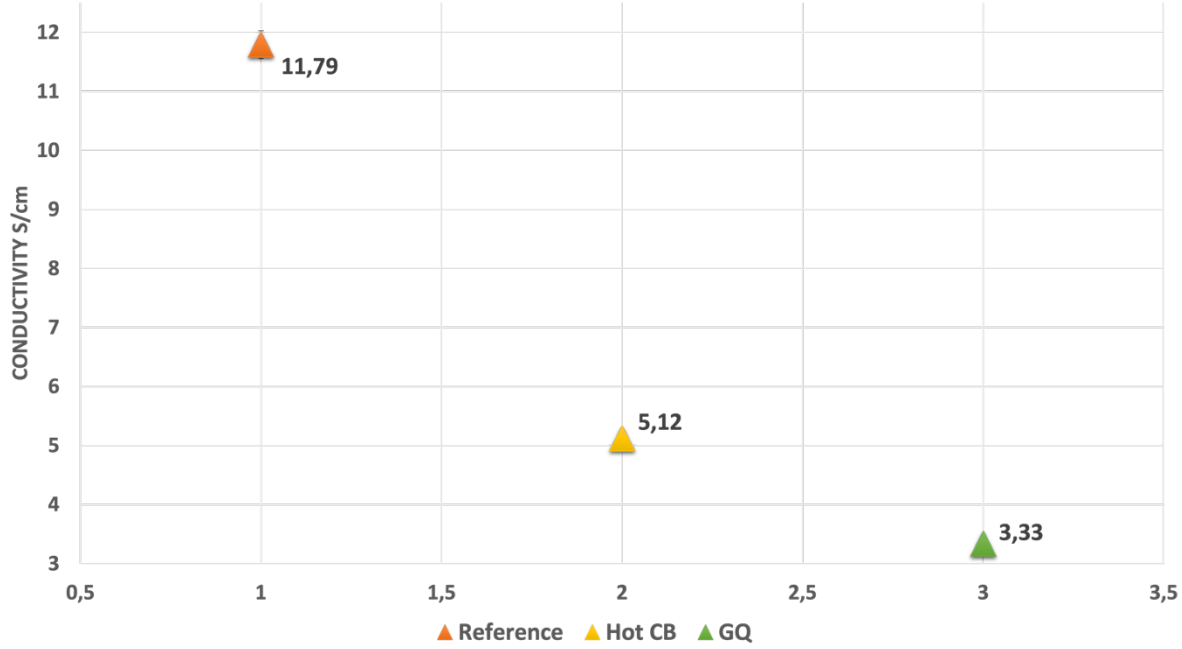

Chart 3 - Conductivity measurement with 4-Point Probe for Film 1M (left) Film 2M (center) Film 3M (right).

- ***Uv-Vis results***

The selected Film 3M that showed the best results in terms of morphology was then tested to characterize the absorption profile in the range of wavelength between 400 – 1000 nm. From the results obtained a band gap of 1.30 eV was obtained, this is consistent with the results that can be found in literature. In this case from photoluminescence measurement the maximum was taken and convert into eV.

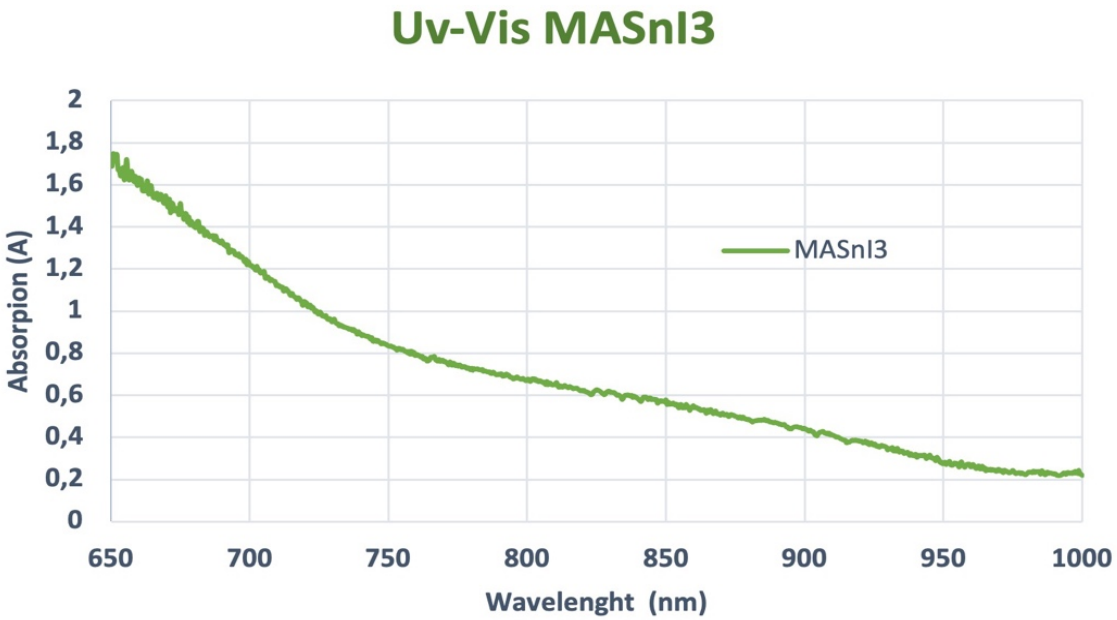

Chart 4 - Uv-Vis measurement for optimized Film 3M

4.5. $CsSnI_3$ film optimisation

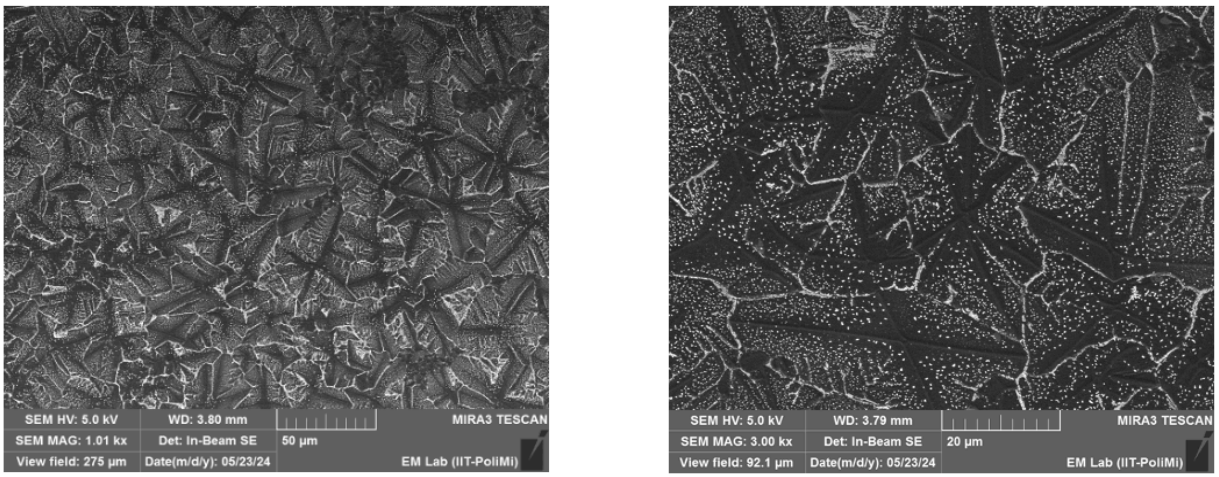

Figure 25 - SEM top view for $CsSnI_3$ Film 1C

The optimization of Cesium Tin Iodide ($CsSnI_3$) films started with the preparation of the precursor solution. Given the inorganic nature of the cesium (Cs) cation, a 4:1 mixture of DMF and DMSO was employed as the solvent but the solution was stirred for 45 minutes at 35°C.

For the fabrication of *Film 1C* (Standard), a standard deposition protocol was followed. This involved spin-coating at 4000 rpm with chlorobenzene as the antisolvent, succeeded by an annealing step at 120°C for 20 minutes. The resulting $CsSnI_3$ film exhibited a distinctive morphology, characterized by leaf-like structures and a notable absence of well-defined grain boundaries. This atypical morphology can likely be attributed to the already reported properties of $CsSnI_3$, which is known to exist in four distinct crystal structures, including a non-perovskite phase stable at room temperature. Furthermore, phase transitions between these structures are readily induced, particularly by temperature variations. In addition to the unusual morphology, small white aggregates were observed on the film surface. These were hypothesized to be undissolved cesium segregating to the top of the film during the fabrication process. In an attempt to enhance grain size, *Film 2C* (hot_CB) was fabricated employing the hot antisolvent technique that worked well for $MASnI_3$ film. While this modification led to the appearance of a few discernible grains, the overall morphology remained largely consistent with that of *Film 1C*, suggesting limited efficacy of this approach for $CsSnI_3$.

A different strategy was adopted for *Film 3C* (Double_Annealing). The precursor solution was stirred for an extended duration of one hour and subsequently filtered to eliminate possible traces of unreacted precursors. This film was fabricated without the use of an antisolvent and subjected to a two-stage annealing process, 20 minutes at 40°C followed by 20 minutes at 80°C. This modified protocol yielded the first $CsSnI_3$ film in this study to exhibit distinct grain formation. No residual cesium was detected on the film surface. Although the grains were relatively small, the film's morphology began to approach those observed with other perovskite cations investigated in this research.

Finally*, Film 4C* (GQ_Annealing 150°) was identified as the optimized film. This film was fabricated utilizing the gas quenching technique during spin-coating. The annealing temperature was increased significantly to 150°C, with the aim of promoting the growth of the small grains observed in *Film 3C*. Considering the high melting point of $CsSnI_3$ (approximately 400°C), no thermal

decomposition of perovskite film was at this elevated temperature. The resulting film exhibited a morphology similar to that of the optimized $MASnI_3$ film (*Film 3M*), characterized by large grains up to 2 mm in size, well-defined grain boundaries, and a minimal presence of pinholes.

Despite the significant morphological improvements achieved with *Film 4C*, the inherent instability of $CsSnI_3$ films remains a critical concern. Even minor exposure to humidity can trigger phase transitions, leading to the formation of the undesirable one-dimensional yellow phase. This sensitivity to ambient conditions presents a substantial challenge to the practical deployment of $CsSnI_3$ - based solar cells.

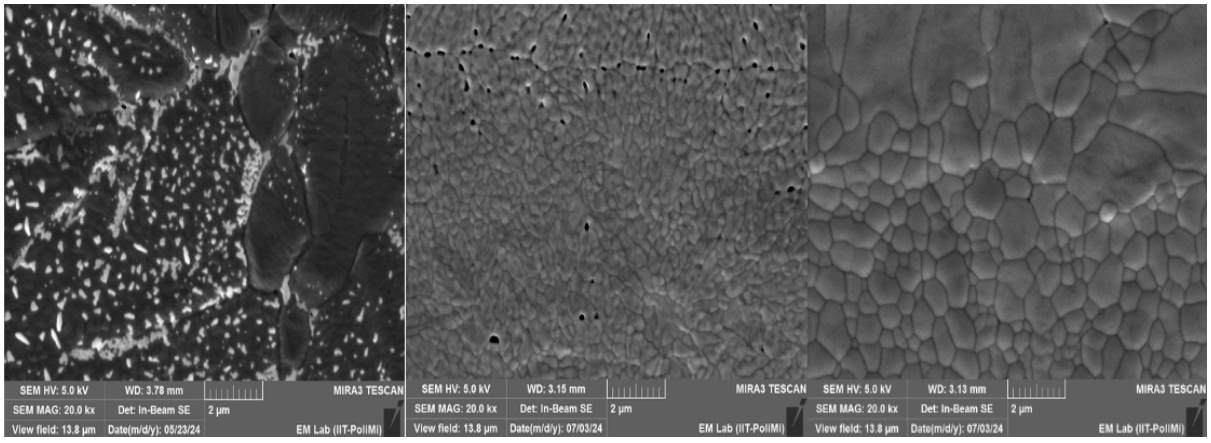

Figure 26 - $CsSnI_3$ samples SEM top view for Film 2C (left), Film 3C (center), Film 4C (left)

- ***XRD measurement***

XRD measurement also in this case were performed and from the results no changes in the crystal structure was noticed. Compared to the $FASnI_3$ and $MASnI_3$ films the peaks identified for $CsSnI_3$ films have similar intensity. The crystal planes represented are peculiar of the orthorhombic and the tetragonal phases that are stable for temperature below 152°C. One comment that could be done regarding the optimized *Film 4C* with gas quenching was that in this case a higher ratio between the 001 and 002 peak was observed. Also in this case a better crystal alignment can be the cause for this shift, since no others substantial differences were observed

Chart 5 - XRD results for film $CsSnI_3$ samples. Film 2C (bottom), Film 3C (middle) , Film 4C (top). 2-Theta scanning angles from 10° to 60°

- ***Four-point probe and Conductivity***

The three selected films were then reproduced on glass substrates to characterize the sheet resistance and from it the conductivity. The measurement was performed within one hour from the end of the spin coating and annealing procedure inside the glovebox thanks to portable four-point probe that was brought inside it. This was done to test fresh films and avoid degradation that can occur even if the film are stored in a N_2 atmosphere. In this case the *Film 2C* was found to have conductivity of 66.36 S/cm that is higher compare to $FASnI_3$ and $MASnI_3$ films. Already from *FILM 3C* a decrease in conductivity to a value of 44.56 S/cm was observed, this could be attribute to the more uniform grains distribution even if small in dimension. The last film was then reported to have conductivity value of 1.06 S/cm comparable with the one measured in $MASnI_3$ and $FASnI_3$. The really good morphology could be one of the reasons for this result.

Unfortunately the result could not be reproduced because on $CsSnI_3$ film produced after this one with homologous procedures resulted to have different structures.

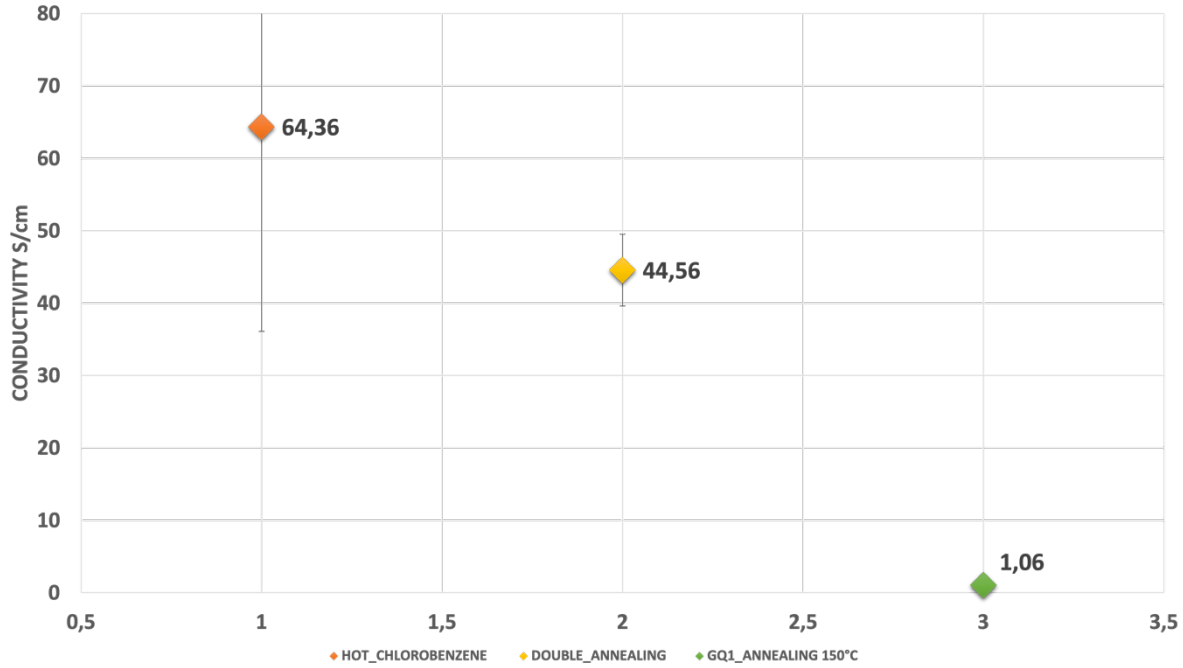

Chart 6 – Conductivity measurement with 4-Point Probe for Film 2C (left) Film 3C (center) Film 4C (right).

- ***Uv-Vis results***

The selected *Film 4C* that showed the better results was then tested to characterize the absorption profile in the range of wavelength between 400 – 1000 nm. From the results obtained a band gap of 1.30 eV was obtained, this respected the result that can be found in literature *[35]*. In this case from photoluminescence measurement the maximum was taken and convert into eV to obtain a approximatively bang gap.

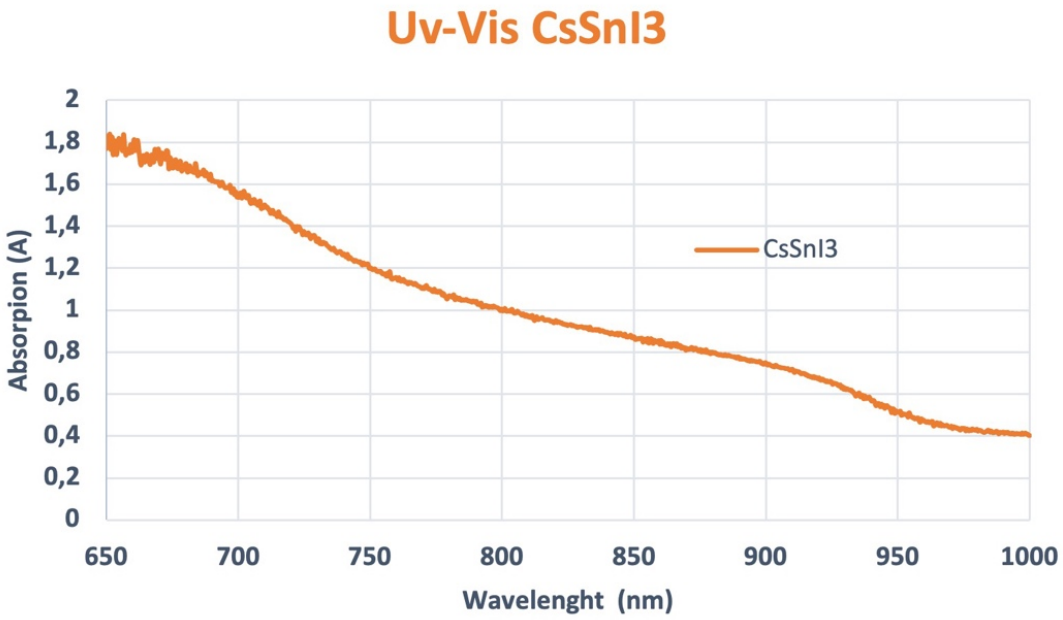

Chart 7 - Uv-Vis measurement for optimized Film 4C

4.6. Hall-Effect results

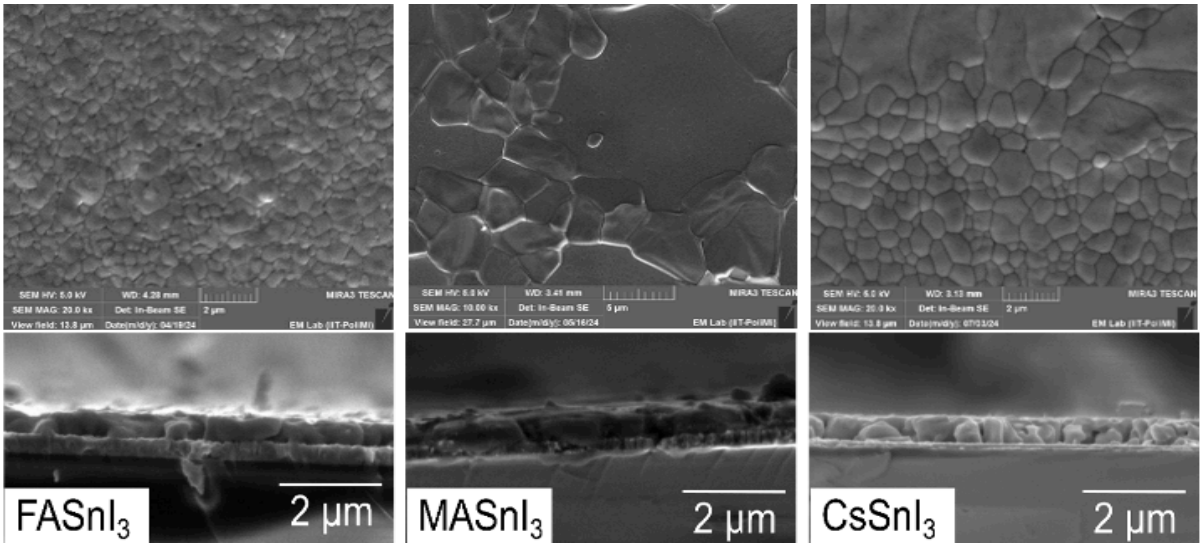

Figure 27 -SEM top views and cross-sections comparison between Film 4F (left), Film 3M (center) and Film 4C (right).

A powerful method to estimate the carriers concentration of the film is the Hall effect measurement. They were obtained using a Hall effect measurement system (HMS5300, Ecopia) using Van Der Pauw method with constant current source and 0.51 Tesla permanent magnet. The device efficiency of tin halide

perovskites is strongly limited by the self-p-doping characteristic of such materials that increase the background hole density to intolerable values of ~10^{19} cm^{-3} *[36]*. P-doping increases recombination rates, reducing dramatically the lifetime and diffusion length of photogenerated charge carriers by more than an order of magnitude compared to the typical values observed in LHPs. The high p-doping can be ascribe to the facile oxidation of Sn^{+2} to Sn^{+4} *[37]*.

The three optimized films (

Figure 27) showed bulk concentration values of 1.56x10^{19}, 8.26x10^{18} and 1.01x10^{19} for $FASnI_3$, $MASnI_3$ and $CsSnI_3$ respectively.

These results show that films with high p-doping characters were obtained, irrespectively of the cation used, suggesting that the cation strongly affects the morphology and structural properties of the material but has limited effect onto the doping nature *[38]*.

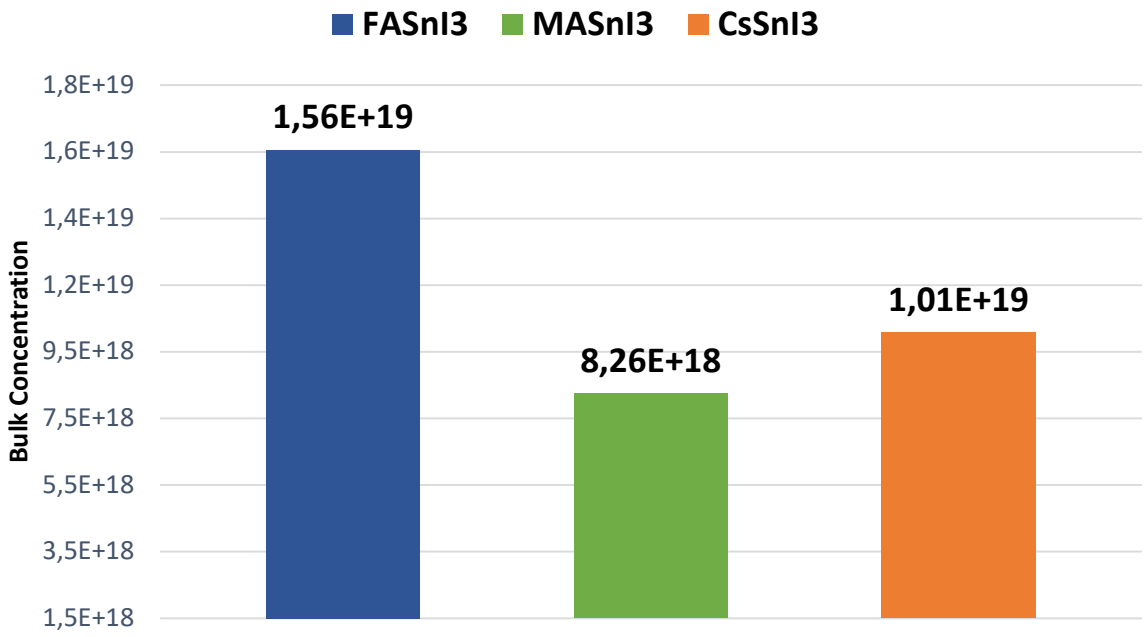

Chart 8 *– Doping density results from Hall Effect measurement for Film 4F , Film 3M and Film 4C*

4.7. Solar cells fabrication

To fully characterize the optimized films working cells were prepared with the p-i-n configuration (details discussed in Perovskite solar cell architecture.

Tin halide perovskite solar cells mainly employed PEDOT:PSS for the deposition of hole transport layer. Unfortunately, PEDOT:PSS is processed from an aqueous solution, which is hardly compatible with the strict anoxic requirement for processing tin halide perovskite due to tin's instability and oxidation. A water free solution was used, containig PEDOT dissolved in toluene. The main problem is that doing that a switch to an hydrophilic situation,when PEDOT:PSS is involve, to a more hydrophobic one, utilizing the water free option, occurred. This fact strongly impacts the substrate properties of the PEDOT layer for perovskite growth make it harder to spread the solution during the spin coating process. Thus we introduced a thin interlayer of Al_2O_3 nanoparticles to modify the wettability of the water-free PEDOT. Despite being an insulator, Al_2O_3 has found application in perovskite PV as an interlayer, nonetheless, the aim was to introduce the smallest amount possible to modify the wetting properties of PEDOT without raising eventual barriers to charge transport. Than as mention above C60, BCP and Silver contact were evaporated on top of the perovskite.

The final cells were then tested in the solar simulator measuring the current output in the range between 1.2V and -0,1V. Direct and reverse scans were performed and the resulting JV curve for optimized $FASnI_3$ cell is shown in figure below .The PCE for the reverse scan was calculated at 0.97 sun of light intensity with a Jsc of 11.92 mA/cm^2 and an Voc 1.11 V of giving the result of 1.11%

For the forward scan instead Jsc of 11,77 mA/cm^2 and an Voc 1.04 V were found giving a PCE results of 1.04%. for $FASnI_3$ pristine film these results were in line with what was found in literature *[39]*.

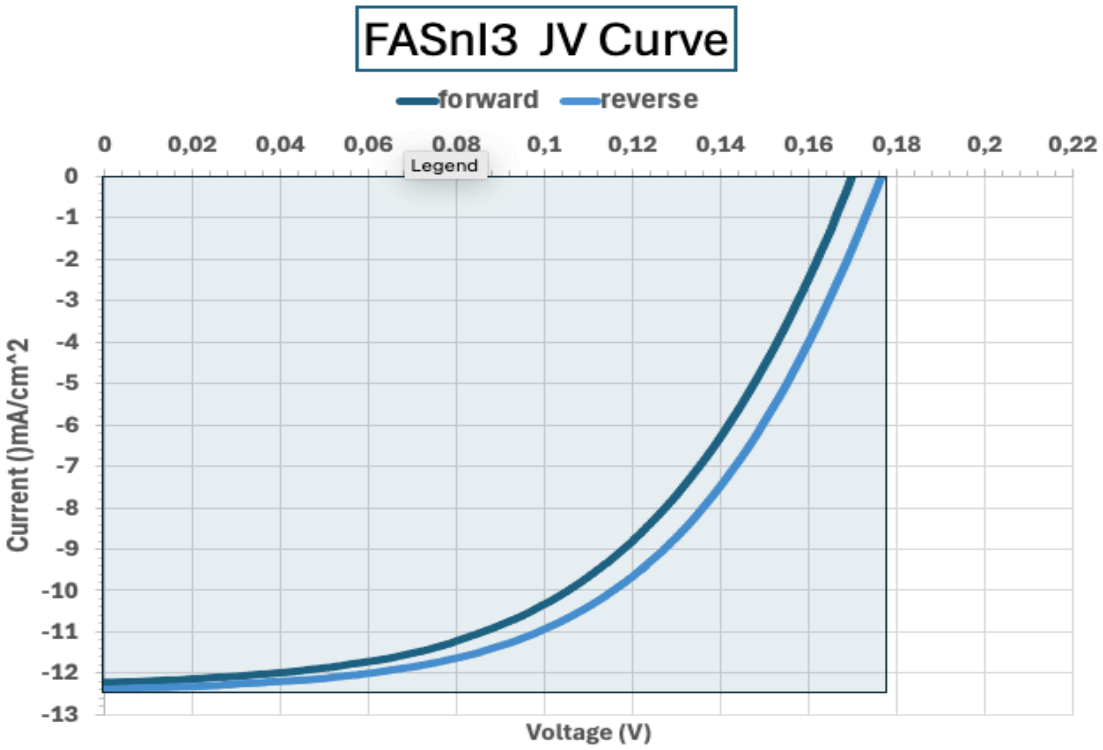

Figure 28 - JV curve for Film 4F solar cell.

The slightly different performance between the reverse and forward scan is commonly referred to as hysteresis. Hysteresis in solar cells refers to a phenomenon where the electrical characteristics of a solar cell depend on the previous history of the voltage or current applied to the cell, rather than just the current conditions. In other words, the J-V curve doesn't retrace exactly the same when the measurement direction is reversed, indicating a lag or delay in the response. In perovskite solar cells it is often attributed to the migration of ions within the perovskite material, which can lead to different electrical characteristics depending on the direction of applied voltage. This phenomena can have impact on the device stability and lifetime moreover it can also reduce the accuracy in reading the PCE measurement.

- ***Cell with additives***

Due to the intrinsic p-doping of THPs cause by Sn spontaneous oxidation many different techniques are still under development to reduce the negative effect that this phenomena has on the properties of the films. Among these, SnF_2 has been the most studied additive used to control the p-doping and improve overall performance. It is wildly used as reducing agent is Sn-based perovskite precursor, its main role is to reduce the oxidation and reduce the doping density and the conductivity of the samples *[40]*. Results show that the addition of 5 to 10 mol % of SnF_2 inside the precursor solution could help reducing fast crystallization rate typical of the THPs and reduce the doping level of the material, however, if the amount of SnF_2 additives is more than 10 mol %, many pinholes appeared on the surface of perovskite thin film and the charge carrier density of thin film will decreased *[41]*. The addition of additives is now a common procedure for the fabrication of efficient solar cell when high Voc, Jv and PCE are needed, since pristine films show very poor performance. The films deposited on PEDOT - Al_2O_3 with the addition of 5 mol % SnF_2 show similar morphology with improve grain size for $FASnI_3$: SnF_2 films. For the $MASnI_3$: SnF_2 film instead the morphology obtained with gas quenching changed from the one obtained without additives. From XRD measurement the crystallinity of the sample is enhance even more that the pristine sample and also the grains show a cubic-alike shape.

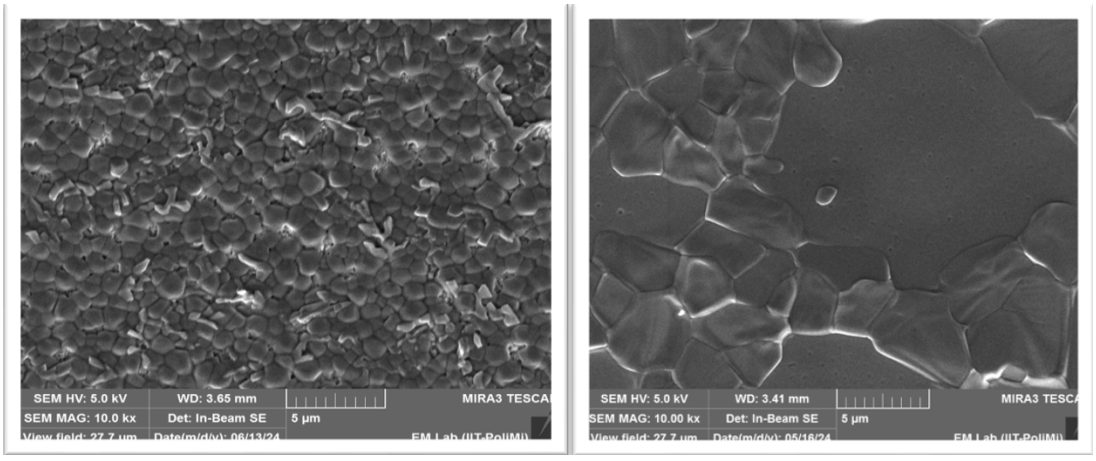

Figure 29 –SEM images for MASnI3 Film 3M with 5% SnF2 (left) and without (right).

As visible from Figure 30 Jsc and Voc have reached higher values when additive were utilized, giving a PCE of 0.59% for the pristine $MASnI_3$ film and 1.40% for the $MASnI_3$ with SnF_2. In conclusion these results were far away from typical PCE values of the tin perovskite solar cells mainly because high performances films are typically prepared utilizing more than one additive and stochiometric mixture of cations, usually FA^+ and Cs^+ *[42][43]*.

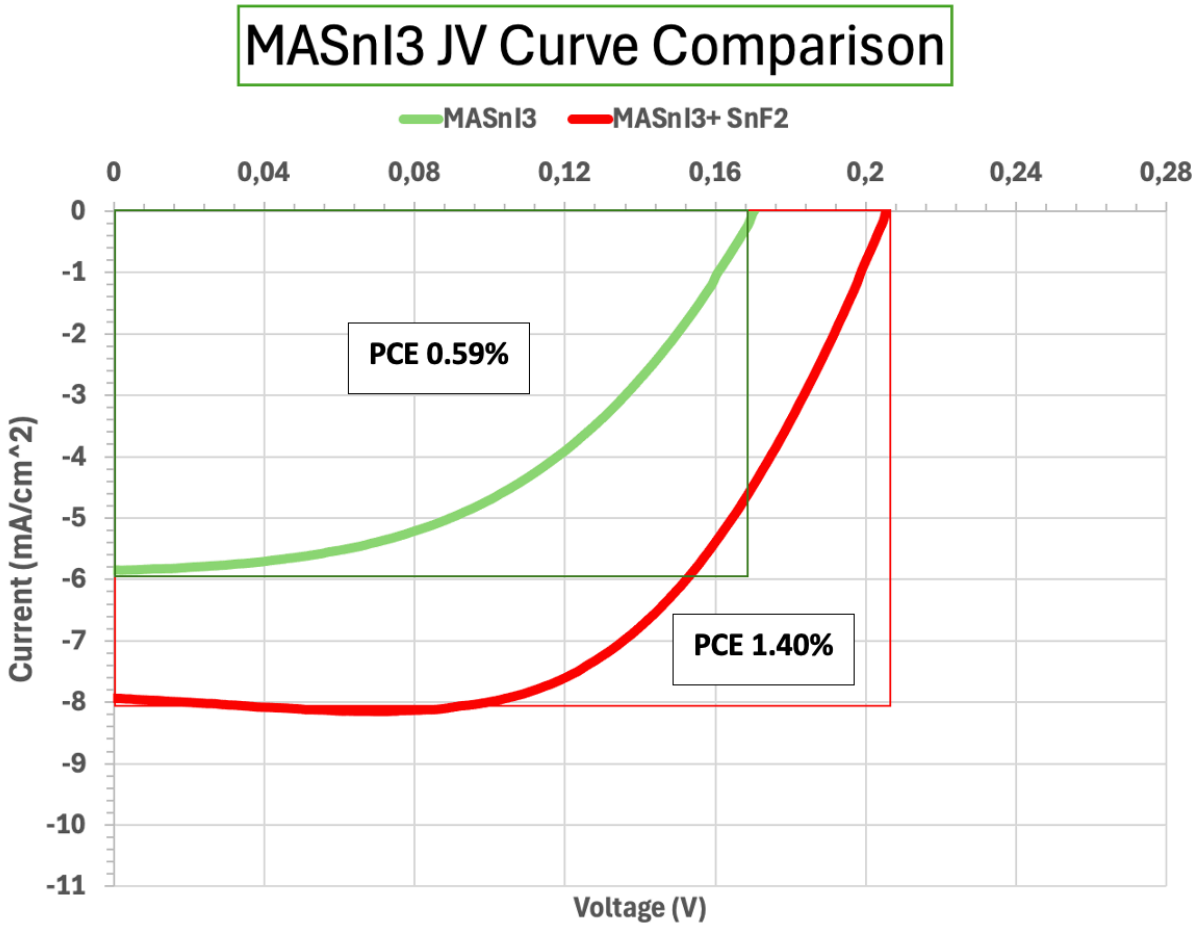

Figure 30 – JV curve for $MASnI_3$ (green) and $MASnI_3$+SnF_2 (red)

5. Conclusion

The aim of this project was to understand the correlation between the films morphology and the optoelectronic proprieties of the pristine perovskite films for FA^+, MA^+ and Cs+ single cations. This could help for further understanding in processing this novel class of materials and define now progresses in producing efficient tin halide solar cells *[44]*.

$FASnI_3$, $MASnI_3$ and $CsSnI_3$ thin films were achieved by spin coating and an optimization of the spin coating technique was carried out to achieve a better film morphology for each of the three cations (pin hole free and fully coverage films). Among the different optimization techniques used, the most effective one was found to be the utilization of a double spin coating rotational speed, which helped achieving a full coverage for the three films eliminating the pin holes that are main cause of poor optoelectronic properties. In addition to this the application of the gas quenching technique was found to gain massive improvements for $MASnI_3$ and $CsSnI_3$ films. The annealing temperature was specifically optimized for each cations to obtain films with distinct grains and the right crystallization. XRD measurement revealed that $MASnI_3$ is the most crystalline material among the three different composition. Uv-vis absorption measurement gave bandgap values in line to what is reported in literature for tin halide perovskite. P-doping levels measurements, taken with an hall effect instrument, showed values in the range of 8 $x10^{18}$ and 1.5 x 10^{19} suggesting that the single cation does not affect the doping level of the material. The conductivity of the samples was also evaluated and an interesting trend in line with the optimization of the films was found, the data suggested that the conductivity decreases in films with smaller grains and full coverage without pin holes. We found that the correlation between the single cation used and the electronic properties of the films are dictated mostly by the films morphology and uniformity rather than the cations intrinsic proprieties itself. Finally, we show that the optimization of the film morphology is not enough to achieve solar cells with high power conversion efficiency. Other techniques in addition to the spin

coating engineering is necessary to reduce the doping level and improve the charge extraction. Additive engineering is the main strategy to decrease tin oxidation and film stability of tin halide perovskites. Finally, a better encapsulation strategy should be engineered to avoid rapid degradation of the perovskite solar cells when exposed to ambient air and allow proper characterization *[45]*.

i. Bibliography

[1] "World Energy Outlook 2022." [Online]. Available: www.iea.org/t&c/

[2] "The Sustainable Development Goals Report Special edition 2023."

[3] K. Calvin *et al.*, "IPCC, 2023: Climate Change 2023: Synthesis Report. Contribution of Working Groups I, II and III to the Sixth Assessment Report of the Intergovernmental Panel on Climate Change [Core Writing Team, H. Lee and J. Romero (eds.)]. IPCC, Geneva, Switzerland.," Jul. 2023. doi: 10.59327/IPCC/AR6-9789291691647.

[4] "https://en.wikipedia.org/wiki/Solar-cell_efficiency".

[5] "NREL. Best research-cell efficiency chart, 2023. URL https://www.nrel.gov/pv/ cell-efficiency.html.".

[6] H. Kang, "Crystalline Silicon vs. Amorphous Silicon: The Significance of Structural Differences in Photovoltaic Applications," in *IOP Conference Series: Earth and Environmental Science*, IOP Publishing Ltd, Apr. 2021. doi: 10.1088/1755-1315/726/1/012001.

[7] "Lu, Kunrun. (2023). Comparison and Evaluation of Different Types of Solar Cells. Applied and Computational Engineering. 23. 263-270. 10.54254/2755-2721/23/20230664. ".

[8] "James M Ball and Annamaria Petrozza. Defects in perovskite - halides and their effects in solar cells. Nature Energy, 1(11):1–13, 2016.".

[9] Y. Rong *et al.*, "Challenges for commercializing perovskite solar cells," Sep. 21, 2018, *American Association for the Advancement of Science*. doi: 10.1126/science.aat8235.

[10] M. Konstantakou and T. Stergiopoulos, "A critical review on tin halide perovskite solar cells," *J Mater Chem A Mater*, vol. 5, no. 23, pp. 11518–11549, 2017, doi: 10.1039/c7ta00929a.

[11] D. Meggiolaro, D. Ricciarelli, A. A. Alasmari, F. A. S. Alasmary, and F. De Angelis, "Tin versus Lead Redox Chemistry Modulates Charge Trapping and Self-Doping in Tin/Lead Iodide Perovskites," *Journal of Physical Chemistry Letters*, vol. 11, no. 9, pp. 3546–3556, May 2020, doi: 10.1021/acs.jpclett.0c00725.

[12] S. Li *et al.*, "Additive engineering for improving the stability of tin-based perovskite (FASnI3) solar cells," Sep. 01, 2022, *Elsevier Ltd*. doi: 10.1016/j.solener.2022.07.009.

[13] R. Tounesi *et al.*, "Influence of A-Site Cation Composition on the Electronic Properties of Halide Tin Perovskites," May 28, 2024, *American Chemical Society*. doi: 10.1021/acsaelm.3c00398.

[14] M. Pitaro, E. K. Tekelenburg, S. Shao, and M. A. Loi, "Tin Halide Perovskites: From Fundamental Properties to Solar Cells," Jan. 01, 2022, *John Wiley and Sons Inc*. doi: 10.1002/adma.202105844.

[15] Y. Wang, J. Liu, J. Wang, and Z. Fan, "Phase Stability and Transformations in CsSnI3: Is Anharmonicity Negligible?," *Journal of Physical Chemistry C*, vol. 126, no. 45, pp. 19470–19479, Nov. 2022, doi: 10.1021/acs.jpcc.2c05775.

[16] M. K. Assadi, S. Bakhoda, R. Saidur, and H. Hanaei, “Recent progress in perovskite solar cells,” Jan. 01, 2018, *Elsevier Ltd*. doi: 10.1016/j.rser.2017.06.088.

[17] M. M. Byranvand, W. Zuo, R. Imani, M. Pazoki, and M. Saliba, “Tin-based halide perovskite materials: properties and applications,” May 23, 2022, *Royal Society of Chemistry*. doi: 10.1039/d2sc01914k.

[18] J. J. Diaz *et al.*, “Analysis of the bonding’s energy in metal-halide perovskites and brief evaluation of meta-GGA functionals TPSS and revTPSS,” *J Mater Sci*, vol. 59, no. 6, pp. 2361–2374, Feb. 2024, doi: 10.1007/s10853-024-09381-2.

[19] S. M. Hasnain, “Examining the advances, obstacles, and achievements of tin-based perovskite solar cells: a review,” Sep. 15, 2023, *Elsevier Ltd*. doi: 10.1016/j.solener.2023.111825.

[20] “Jiang Q, Tong J, Xian Y, Kerner RA, Dunfield SP, Xiao C, Scheidt RA, Kuciauskas D, Wang X, Hautzinger MP, Tirawat R, Beard MC, Fenning DP, Berry JJ, Larson BW, Yan Y, Zhu K. Surface reaction for efficient and stable inverted perovskite solar cells. Nature. 2022 Nov;611(7935):278-283. doi: 10.1038/s41586-022-05268-x. Epub 2022 Sep 1. PMID: 36049505.”.

[21] T. Li, F. He, J. Liang, and Y. Qi, “Functional layers in efficient and stable inverted tin-based perovskite solar cells,” Sep. 20, 2023, *Cell Press*. doi: 10.1016/j.joule.2023.08.002.

[22] D. Di Girolamo *et al.*, “Enabling water-free PEDOT as hole selective layer in lead-free tin perovskite solar cells,” *Mater Adv*, vol. 3, no. 24, pp. 9083–9089, 2022, doi: 10.1039/D2MA00834C.

[23] B. Chen, S. Wang, X. Zhang, W. Zhu, Z. Cao, and F. Hao, “Reducing the interfacial voltage loss in tin halides perovskite solar cells,” *Chemical Engineering Journal*, vol. 445, Oct. 2022, doi: 10.1016/j.cej.2022.136769.

[24] S. Liu, V. P. Biju, Y. Qi, W. Chen, and Z. Liu, “Recent progress in the development of high-efficiency inverted perovskite solar cells,” Dec. 01, 2023, *Nature Research*. doi: 10.1038/s41427-023-00474-z.

[25] S. Ahmed, M. A. Gondal, A. S. Alzahrani, M. Parvaz, A. Ahmed, and S. Hussain, “Recent Trends and Challenges in Lead-Free Perovskite Solar Cells: A Critical Review,” Feb. 26, 2024, *American Chemical Society*. doi: 10.1021/acsaem.3c02327.

[26] P. Mahajan, R. Datt, W. Chung Tsoi, V. Gupta, A. Tomar, and S. Arya, “Recent progress, fabrication challenges and stability issues of lead-free tin-based perovskite thin films in the field of photovoltaics,” Feb. 15, 2021, *Elsevier B.V.* doi: 10.1016/j.ccr.2020.213633.

[27] G. F. Harrington and J. Santiso, “Back-to-Basics tutorial: X-ray diffraction of thin films,” *J Electroceram*, vol. 47, no. 4, pp. 141–163, Dec. 2021, doi: 10.1007/s10832-021-00263-6.

[28] “Poli_Cation Sn_manuscript”.

[29] S. Saini *et al.*, “Use of anti-solvent to enhance thermoelectric response of hybrid halide perovskite thin films,” *Jpn J Appl Phys*, vol. 61, no. SE, Jun. 2022, doi: 10.35848/1347-4065/ac4adb.

[30] M. Ozaki *et al.*, “Solvent-coordinated tin halide complexes as purified precursors for tin-based perovskites,” *ACS Omega*, vol. 2, no. 10, pp. 7016–7021, Oct. 2017, doi: 10.1021/acsomega.7b01292.

[31] A. Bouich, J. Marí-Guaita, B. M. Soucase, and P. Palacios, “Manufacture of High-Efficiency and Stable Lead-Free Solar Cells through Antisolvent Quenching Engineering,” *Nanomaterials*, vol. 12, no. 17, Sep. 2022, doi: 10.3390/nano12172901.

[32] L. Wang *et al.*, “Annealing Engineering in the Growth of Perovskite Grains,” Jul. 01, 2022, *MDPI*. doi: 10.3390/cryst12070894.

[33] S. J. Yang, J. Choi, S. Song, C. Park, and K. Cho, “Enhancing air-stability and reproducibility of lead-free formamidinium-based tin perovskite solar cell by chlorine doping,” *Solar Energy Materials and Solar Cells*, vol. 227, Aug. 2021, doi: 10.1016/j.solmat.2021.111072.

[34] X. Meng *et al.*, “Surface-Controlled Oriented Growth of FASnI3 Crystals for Efficient Lead-free Perovskite Solar Cells,” *Joule*, vol. 4, no. 4, pp. 902–912, Apr. 2020, doi: 10.1016/j.joule.2020.03.007.

[35] I. Chung *et al.*, “CsSnI 3: Semiconductor or metal? High electrical conductivity and strong near-infrared photoluminescence from a single material. High hole mobility and phase-transitions,” *J Am Chem Soc*, vol. 134, no. 20, pp. 8579–8587, May 2012, doi: 10.1021/ja301539s.

[36] Mario Caironi, Isabella Poli, and Paolo Giavarini, “Thermoelectric properties and self-doping mechanisms of halide perovskites,” 2021.

[37] A. Treglia *et al.*, “Effect of electronic doping and traps on carrier dynamics in tin halide perovskites,” *Mater Horiz*, vol. 9, no. 6, pp. 1763–1773, Apr. 2022, doi: 10.1039/d2mh00008c.

[38] “Yukari Takahashi, Hiroyuki Hasegawa, Yukihiro Takahashi, Tamotsu Inabe, Hall mobility in tin iodide perovskite CH3NH3SnI3: Evidence for a doped semiconductor, Journal of Solid State Chemistry, Volume 205, 2013, Pages 39-43, ISSN 0022-4596.”.

[39] W. Ke *et al.*, “Enhanced photovoltaic performance and stability with a new type of hollow 3D perovskite {en}FASnI3,” *Sci Adv*, vol. 3, no. 8, p. e1701293, Dec. 2024, doi: 10.1126/sciadv.1701293.

[40] M. Dawson, C. Ribeiro, and M. R. Morelli, “A Review of Three-Dimensional Tin Halide Perovskites as Solar Cell Materials,” 2022, *Universidade Federal de Sao Carlos*. doi: 10.1590/1980-5373-MR-2021-0441.

[41] S. Gupta, D. Cahen, and G. Hodes, “How SnF2 Impacts the Material Properties of Lead-Free Tin Perovskites,” *Journal of Physical Chemistry C*, vol. 122, no. 25, pp. 13926–13936, Jun. 2018, doi: 10.1021/acs.jpcc.8b01045.

[42] A. K. Singh, S. Srivastava, A. Mahapatra, J. K. Baral, and B. Pradhan, “Performance optimization of lead free-MASnI3 based solar cell with 27% efficiency by numerical

simulation,” *Opt Mater (Amst)*, vol. 117, p. 111193, 2021, doi: https://doi.org/10.1016/j.optmat.2021.111193.

[43] F. J. Berger *et al.*, “How Halide Alloying Influences the Optoelectronic Quality in Tin-Halide Perovskite Solar Absorbers,” *ACS Energy Lett*, vol. 8, no. 9, pp. 3876–3882, Sep. 2023, doi: 10.1021/acsenergylett.3c01241.

[44] B. Salhi, Y. S. Wudil, M. K. Hossain, A. Al-Ahmed, and F. A. Al-Sulaiman, “Review of recent developments and persistent challenges in stability of perovskite solar cells,” Jul. 01, 2018, *Elsevier Ltd*. doi: 10.1016/j.rser.2018.03.058.

[45] E. Aktas *et al.*, “Challenges and strategies toward long-term stability of lead-free tin-based perovskite solar cells,” Dec. 01, 2022, *Springer Nature*. doi: 10.1038/s43246-022-00327-2.

ii. Acknowledgements

E quindi alla fine eccoci qua!! Finisce un capito della mia vita fatto di molte emozioni e moltiiii pensieri, di alti e bassi, conferme e delusioni, come è di per sé l’università. Tutto questo non sarebbe stato di certo possibile se non fosse per alcune persone che ci terrei a ringraziare.
In primis vorrei ringraziare me stesso,
fine!!

No scherzo dai, non voglio sembrare troppo eccentrico, un ringraziamento va a Isabella per avermi sopportato sei mesi a IIT e avermi guidato con la sua esperienza in questa tesi e avermi fatto conoscere meglio questo complicato mondo delle perovskiti , e in generale un grazie a tutti i colleghi di laboratorio che mi hanno aiutato nella realizzazione di questo progetto. Un grazie anche a Prof. Daniele che mi ha aperto un sacco di porte grazie alle sue conoscenze e alla suadisponibilità. Un grande grazie a i miei colleghi di corso, Pietro, Gianmarco, Luigi , Natasha e Rebecca di corso con cui ho condiviso questo percorso e molto di più, tra serate a girovagare per Bologna. Alcool a basso costo della Pam e vacanze estive che sicuramente avranno un posto speciale nei miei ricordi. Un grazie a Camilla, non so bene per cosa a dire il vero, penso che dire per tutto sia riduttivo. Grazie per le giornate passate in Unione a preparare gli esami da mattina a sera, grazie per avermi fatto perdere un sacco di lezioni perché alzarsi dal letto era una fatica (non ho mai opposto resistenza), grazie per aver reso questa esperienza da fuorisede meno "sede" e più "fuori" con la tua solarità, il tuo splendido sorriso e la tua "pazzia" latente. Grazie per avermi sempre spronato e fatto sentire pronto e all'altezza di poter affrontare tutto, il tuo sostegno è stato fondamentale durante questi due anni.
Mamma passiamo a te!! Che dirti , vedi che alla fine anche senza che mi rimproveri sempre le cose le riesco a fare anche da solo!!! Grazie di sopportarmi e, a modo tuo, supportarmi e spronarmi sempre, grazie per le tonnellate di cibo che mi hai fornito durante questi due anni, senza di te sarei anche anoressico

oltre che “quasi” calvo. Spero che vedermi con una corona d’ alloro non una ma ben due volte ti faccia capire che tutti gli sforzi e le incazzature che ci siamo fatti , per i compiti a casa, per i 5- (quando andava bene) a scuola e per le pagelle non sempre delle migliori, in fin dei conti serviti a qualcosa.

Hai cresciuto un fiorellino di uomo educato, gentile e premuroso proprio come te, ma proprio come te anche testardo e permaloso ed a farne le spese aimè sei stata tu che ci sei sempre stata in ogni momento soprattutto quando avevo più bisogno. So tutti gli sforzi che fai per me, e non solo per me, prometto che imparerò a darti il rispetto che meriti. Anche se non spesso te lo dico e anche se quando te lo dico pensi sempre sia perché mi serve qualcosa, ti voglio bene mamma!! E poi dall’altra parte della medaglia ci sei tu papà, che di come andassi a scuola te ne fregava poco e niente se non quando te lo imponeva mamma, perché da te ho imparato che non tutto si impara sui libri anzi, quasi nulla e che nei momenti passati insieme mi hai insegnato tutto quello che per un vero uomo cosa davvero conta nella vita. Sei il Professore in Tuttologia che l’università non avrà mai. Se ora sono qui a Singapore lo devo a te, e non parlo dei finanziamenti che mi hai dato. Grazie per aver sostenuto i miei studi ma soprattutto per tutte le esperienze che mi hanno permesso di fare e che mi hanno fatto diventare chi sono oggi.

Se da un lato di questa medaglia chiamata famiglia ho la fortuna di avere una mamma che vale due dall’altro ho trovato un papà che vale come migliore amico.

Un’ altro grazie speciale alla Zia Alessandra, perché se oggi sono un maestro del computer è solo grazie a tutte le cose che mi ha chiesto di farle in questi anni. Il tuo nipotino ti vuole bene a ti aiuterà sempre, più o mendo indisposto a seconda delle giornate. Un saluto al nonno Gino che ogni volta che gli parlo di università mi fa sentire come se stessi diventando presidente degli Stati Uniti d’America e mi convinco che sto andando alla grande e che grandi cose mi attendono sul mio cammino. Un bacio grande al mio angelo custode, che sicuramente in questo momento sarà fiera di me e si starà vantando con tutti di

quando è formidabile in suo nipotino. Ciao nonna, so che mi accompagni e mi guidi in ogni cosa che faccio.

Un abbraccio e un grazie a tutti gli amici, troppi da elencare uno ad uno, con cui ho condiviso tutto quanto dai momenti più felici a quelli aimè tristi. Come mi diverto con voi non mi diverto con nessuno e anche quando le cose si fanno dure e stressanti sò che su di voi posso sempre contare per svuotare la mente. Finalmente ora non avrò più l’etichetta dell’ “UniLife”, vi raggiungo nella vita vera.
A ripensarci forse potevo prendermela un po’ più comoda nel laurearmi!!!

E infine un grazie a ME per aver portato a termine questo corso di laurea, perché su, parliamoci chiaro, non avete mica fatto voi per me tutti sti esami belin!!